Since January 2020 Elsevier has created a COVID-19 resource centre with free information in English and Mandarin on the novel coronavirus COVID-19. The COVID-19 resource centre is hosted on Elsevier Connect, the company's public news and information website.

Expert Systems With Applications 185 (2021) 115637

Contents lists available at ScienceDirect

Expert Systems With Applications

journal homepage: www.elsevier.com/locate/eswa

A quantum-clustering optimization method for COVID-19 CT scan image segmentation

Pritpal Singh [a,*,1], Surya Sekhar Bose [b,1]

[a] Institute of Theoretical Physics, Jagiellonian University, ul.Łojasiewicza 11, Kraków 30-348, Poland
[b] Department of Mathematics, Madras Institute of Technology, MIT Rd, Radha Nagar, Chromepet, Chennai, Tamil Nadu 600044, India

ARTICLE INFO

Keywords:
Coronavirus Disease 2019 (COVID-19)
K-means clustering (KMC) algorithm
Fast forward quantum optimization algorithm (FFQOA)
Computed tomography (CT) images
Image segmentation

ABSTRACT

The World Health Organization (WHO) has declared Coronavirus Disease 2019 (COVID-19) as one of the highly contagious diseases and considered this epidemic as a global health emergency. Therefore, medical professionals urgently need an early diagnosis method for this new type of disease as soon as possible. In this research work, a new early screening method for the investigation of COVID-19 pneumonia using chest CT scan images has been introduced. For this purpose, a new image segmentation method based on K-means clustering algorithm (KMC) and novel fast forward quantum optimization algorithm (FFQOA) is proposed. The proposed method, called FFQOAK (FFQOA+KMC), initiates by clustering gray level values with the KMC algorithm and generating an optimal segmented image with the FFQOA. The main objective of the proposed FFQOAK is to segment the chest CT scan images so that infected regions can be accurately detected. The proposed method is verified and validated with different chest CT scan images of COVID-19 patients. The segmented images obtained using FFQOAK method are compared with various benchmark image segmentation methods. The proposed method achieves mean squared error, peak signal-to-noise ratio, Jaccard similarity coefficient and correlation coefficient of 712.30, 19.61, 0.90 and 0.91 in case of four experimental sets, namely Experimental_Set_1, Experimental_Set_2, Experimental_Set_3 and Experimental_Set_4, respectively. These four performance evaluation metrics show the effectiveness of FFQOAK method over these existing methods.

1. Introduction

In late 2019, the novel COVID-19 pneumonia was observed in Wuhan City, China (Cohen & Normile, 2020; Zhu et al., 2020). Huang et al. (2020) identified the typical manifestation symptoms of COVID-19 based on 41 patients in Wuhan city, which included fever, cough, myalgia and fatigue. All of these 41 patients suffered from pneumonia and showed abnormalities in their chest computed tomography (CT). These patients also had serious health problems that included acute respiratory illness, acute cardiac injury, and secondary infections. Of these, 13 patients were transferred to the Intensive Care Unit (ICU), while 6 patients died during the course of treatment. For the first time, Chan and colleagues (Chan et al., 2020) had found evidence of human-to-human spread COVID-19 disease at the Hong Kong University.

COVID-19 is associated with severe respiratory symptoms leading to ICU admissions and death with high frequency (Katris, 2021; Zhou et al., 2020). The type of pneumonia caused by COVID-19 is a highly infectious disease and this outbreak has been declared a global public health emergency by the WHO (WHO, 2020). A real-time RT-PCR approach was used to diagnose COVID-19 pneumonia, which indicated positive symptoms of severe acute respiratory syndrome coronavirus 2 in nine pregnant women (Chen et al., 2020). However, in the case of COVID-19 infection, the RT-PCR approach has a very low positive rate and may not be effective for early detection and treatment of suspected patients (Fang et al., 2020). Nevertheless, medical imaging technologies, such as X-ray, CT, magnetic resonance imaging (MRI), etc. have made a significant contribution to improve diagnostic accuracy, timeliness, and performance (Nowaková, Prílepok, & Snášel, 2017). A recent study shows that certain features associated with COVID-19 can be detected in the lungs by chest CT image (Chung et al., 2020). Li et al. (2020) have used a deep learning approach to separate COVID-19 from all other viral pneumonias based on CT chest examinations. Such studies (Chung et al., 2020; Li et al., 2020) have shown that CT could be an effective tool for early COVID-19 testing and diagnosis. Notwithstanding the advantages of CT scanning, these images share some common image features between COVID-19 and

* Corresponding author.
E-mail addresses: drpritpalsingh82@gmail.com (P. Singh), sbose499@yahoo.com (S.S. Bose).
[1] All authors contributed equally to this article.

https://doi.org/10.1016/j.eswa.2021.115637
Received 17 November 2020; Received in revised form 25 April 2021; Accepted 18 July 2021
Available online 28 July 2021

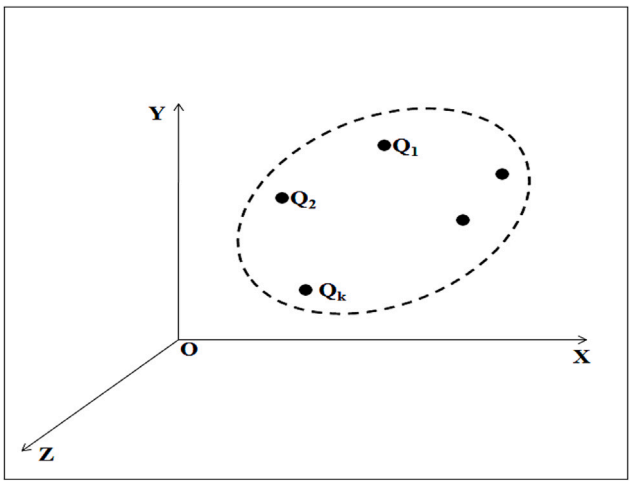

Fig. 1. A quantum system with q number of quanta Q_k $(k = 1, 2, \ldots, q)$.

other types of pneumonia that make it very difficult to distinguish between them. Such features can therefore be distinguished in terms of similarities and dissimilarities using various image processing methods.

Image segmentation is one of the tedious tasks in image processing and pattern recognition, with many applications in computer vision, robotics, object recognition, and so on. The main purpose of image segmentation is to separate each object in the image from the rest of the artifacts (Tobias & Seara, 2002). Thus, it is a mechanism for dividing an image into different parts so that each part has its own region. According to Cheng, Jiang, Sun, and Wang (2001), it is a method of partitioning an image I into non-overlapping regions $(I_1, I_2, \ldots, I_n)$ such that:

$$\bigcup_{i}^{n} I_i = I, \text{and } I_i \cap I_j = \emptyset, I_i \neq I_j \tag{1}$$

Image segmentation is a tedious mechanism due to the involvement of complexities related to contrast, brightness, noise, etc. (Yang, Zhao, Chen, & Fang, 2008). In segmentation, some issues always arise such as:

1. How to distinguish objects from each other, since they often overlap in color?
2. How to distinguish objects from the background, because their color levels may be similar?
3. How to adequately quantify color levels so that certain objects belong to a specific set?

Many image segmentation methods have been proposed to address these issues, including the Otsu thresholding method (Xu, Xu, Jin, & Song, 2011), the multilevel thresholding method (Manikandan, Ramar, Iruthayarajan, & Srinivasagan, 2014), the watershed method (Cates, Whitaker, & Jones, 2005), the adaptive thresholding method (Issac, Sarathi, & Dutta, 2015), the ambiguous set based segmentation method (Singh, Huang, & Lee, 2019), the neutrosophic-entropy based clustering algorithm (Singh, 2020b), the neutrosophic-entropy based adaptive thresholding segmentation algorithm (Singh, 2020a), the fuzzy-entropy-fusion based thresholding method (Singh, Huang, Chu, & Lee, 2020) and the multiple thresholding method (Singh, 2021b). These methods used specific thresholds to distinguish the objects and have been successfully used in medical image segmentation. Some of the existing segmentation methods (Gordillo, Montseny, & Sobrevilla, 2013; Kong et al., 2020; Menze et al., 2014) are based on partitioning medical images by identifying discontinuous color levels in a given region. While these methods are computationally simple and inexpensive, they are very sensitive to threshold selection.

One of the most popular methods is the KMC algorithm (Queen, 1967), which assigns each color level to the respective cluster depending on certain distance criteria (Yao, Duan, Li, & Wang, 2013). However, the KMC algorithm has the following inherent drawbacks (Selim & Ismail, 1984):

- It is observed that the KMC algorithm generates many cluster centers with local optima and often misses the global optima.
- The optimal results of the KMC algorithm are very sensitive to the initial definition of the cluster centers. It is observed that different clusters can be generated with different initial cluster centers.

Many improved methods are proposed by hybridizing the following optimization algorithms to overcome the above drawbacks of KMC algorithm. These methods are given in the following list:

- Genetic Algorithm (GA)+ KMC=GAK (Khrissi, Akkad, Satori, & Satori, 2020),
- Particle Swarm Optimization (PSO)+ KMC=PSOK (van der Merwe & Engelbrecht, 2003),
- Dynamic PSO (DPSO)+ KMC=DPSOK (Li, He, & Wen, 2015), and
- Ant Colony Optimization (ACO)+ KMC=ACOK (Saatchi & Hung, 2005).

However, such hybridization of optimization algorithms is either too difficult or only partially overcomes the drawbacks of the KMC algorithm. This shows the need for further studies to solve the problems of the KMC algorithm, especially towards solving the problems of optimal cluster centers and global optima. Through this motivation, this study proposed a novel FFQOA, which is the updated version of the existing quantum optimization algorithm (QOA) (Singh, Dhiman, & Kaur, 2018) and modified QOA (MQOA) (Huang, Singh, Kuo, & Chu, 2021). However, these algorithms have certain weaknesses, such as:

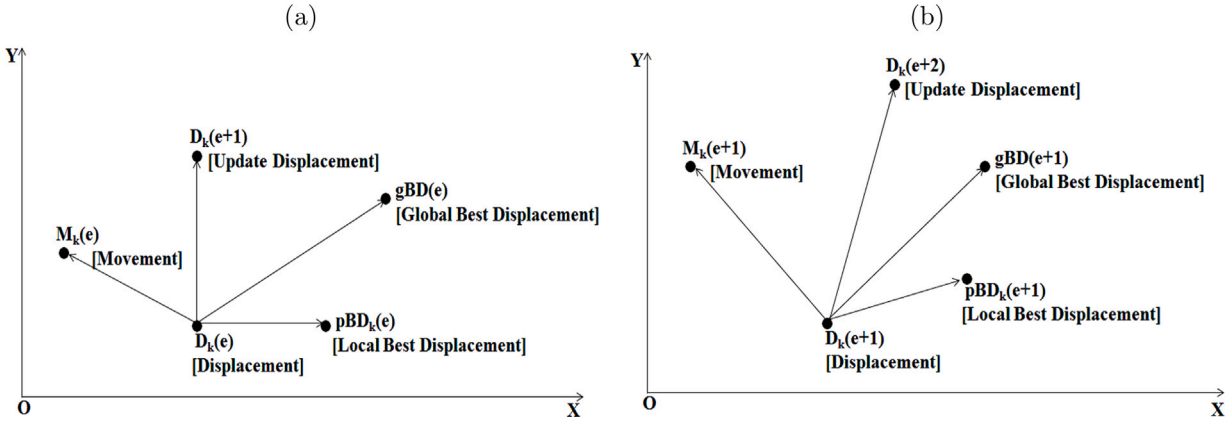

Fig. 2. A two-dimensional geometrical representation of movement and displacement enhancements for a quantum: (a) at epoch e, and (b) at epoch $e + 1$.

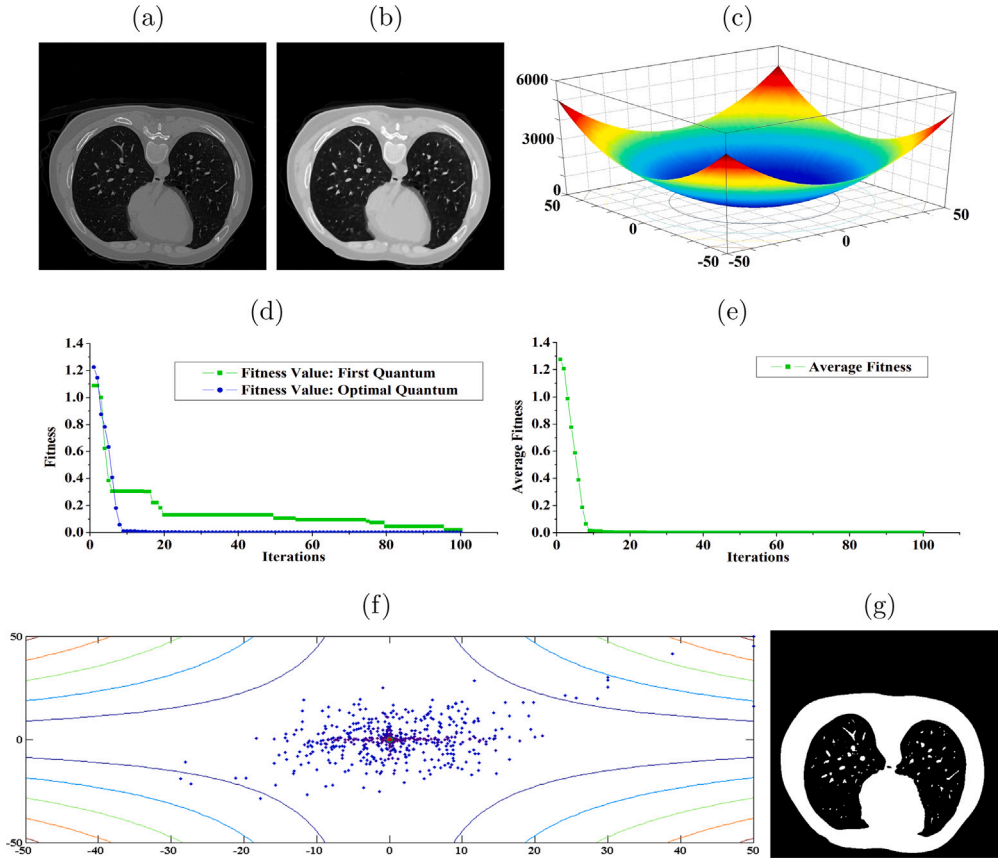

Fig. 3. Searching processes of the proposed FFQOAK during segmentation: (a) CT scan image of COVID-19, (b) enhanced CT scan image of (a), (c) search landscape, (d) comparison of fitness, (e) average fitness curve, (f) search history, and (g) segmented image of (b).

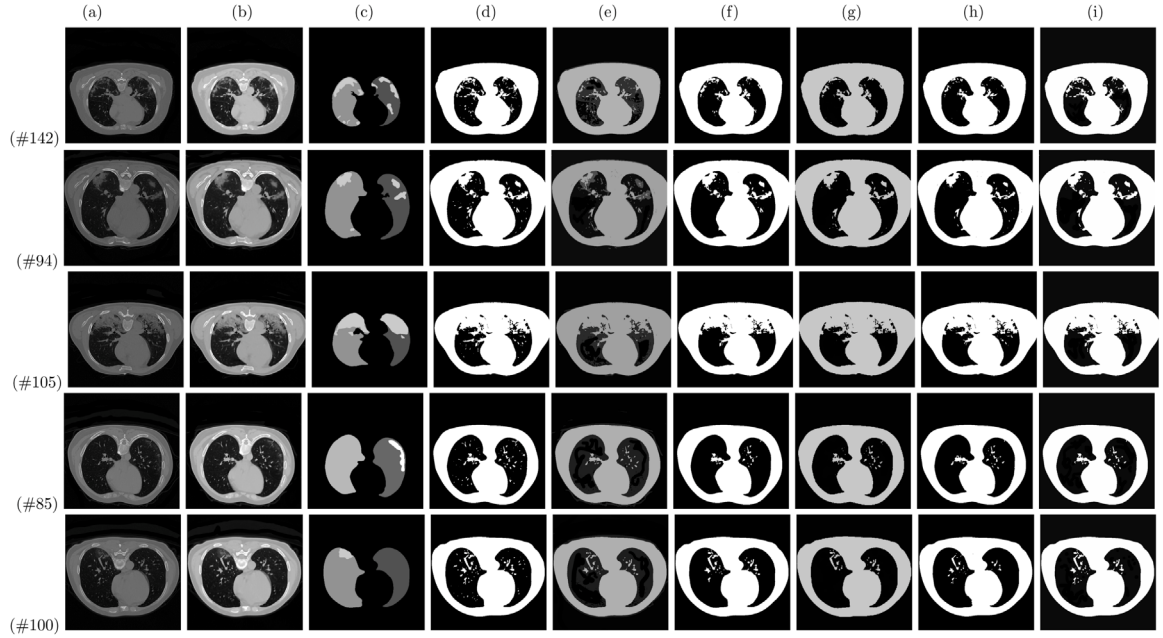

Fig. 4. Segmentation of CT scan images of Experimental_Set_1 (Case labels: 1–5) of COVID-19 using the proposed FFQOAK and existing methods: (a) extracted CT scan image, (b) enhanced CT scan image of (a), (c) GT of (a), (d) proposed FFQOAK, (e) KMC, (f) GAK, (g) PSOK, (h) DPSOK, and (i) ACOK.

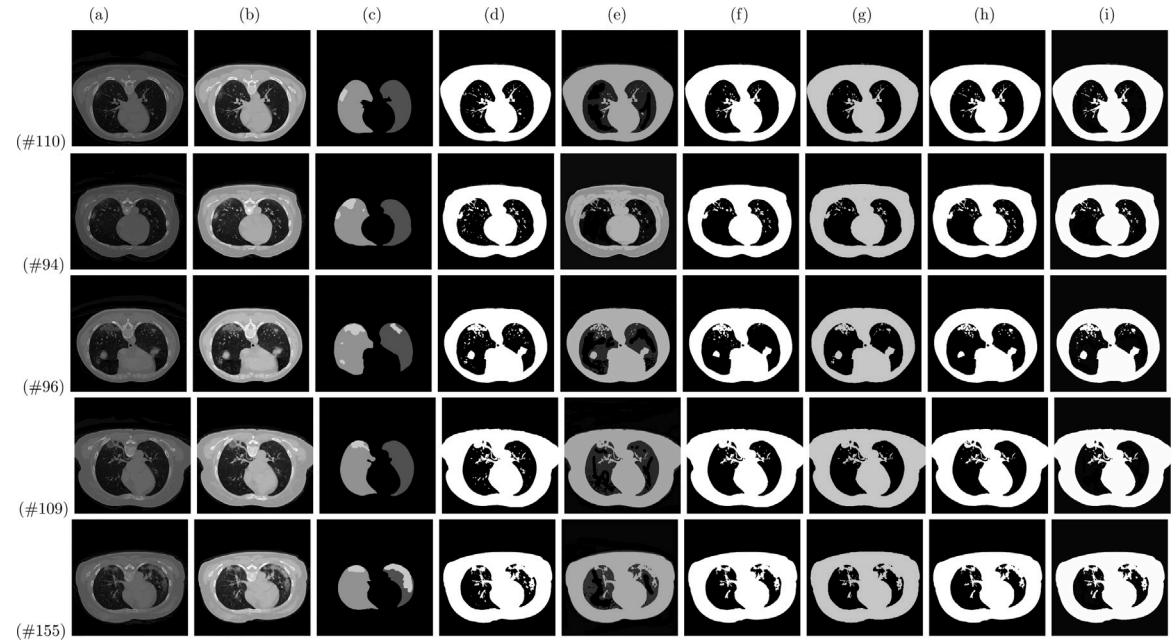

Fig. 5. Segmentation of CT scan images of Experimental_Set_1 (Case labels: 6–10) of COVID-19 using the proposed FFQOAK and existing methods: (a) extracted CT scan image, (b) enhanced CT scan image of (a), (c) GT of (a), (d) proposed FFQOAK, (e) KMC, (f) GAK, (g) PSOK, (h) DPSOK, and (i) ACOK.

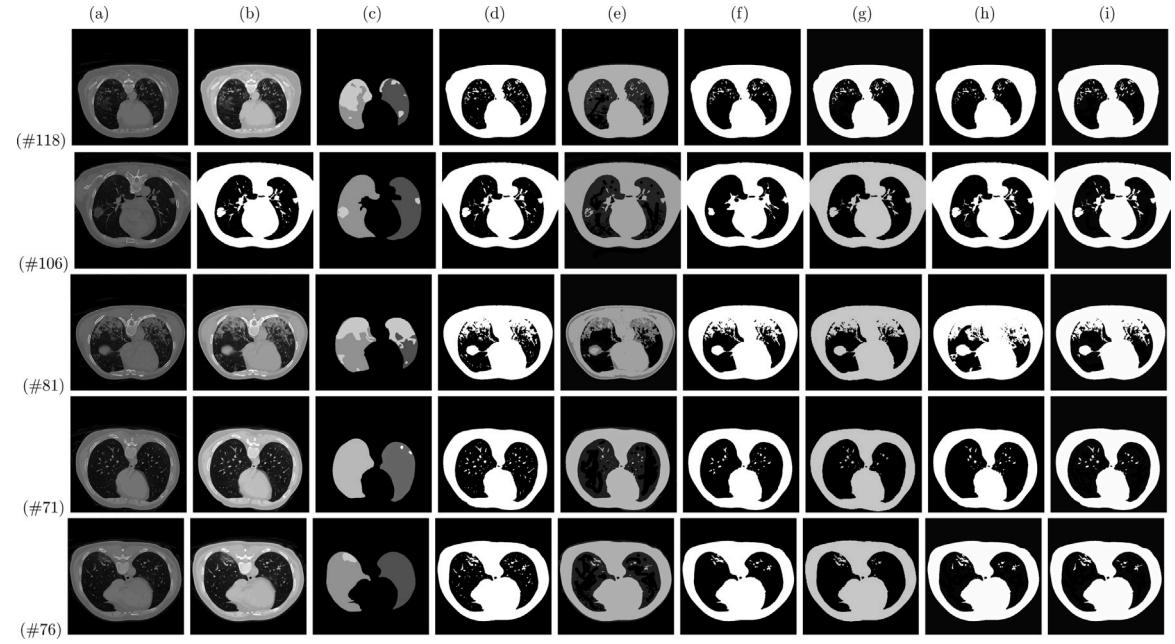

Fig. 6. Segmentation of CT scan images of Experimental_Set_2 (Case labels: 1–5) of COVID-19 using the proposed FFQOAK and existing methods: (a) extracted CT scan image, (b) enhanced CT scan image of (a), (c) GT of (a), (d) proposed FFQOAK, (e) KMC, (f) GAK, (g) PSOK, (h) DPSOK, and (i) ACOK.

- A well-defined formulation of the quantum system that serves as a set of search agents to find the optimal global solution is not properly defined.
- There is no description of appropriate ranges for the various constants.
- There is no consideration of the locally and globally optimal values for finding the optimal solution.

Significant improvements are made to the QOA and MQOA as part of this research, which have been incorporated into the FFQOA. These are listed as:

- Well-defined ranges for the constants and parameters are given.
- Formulations for the quantum system are properly defined.
- Formulas for initializing the quantum's location, movement and displacement in the quantum system are included.
- Mechanisms for enhancing the search scope and updating the displacement are included. For this purpose, the FFQOA considers

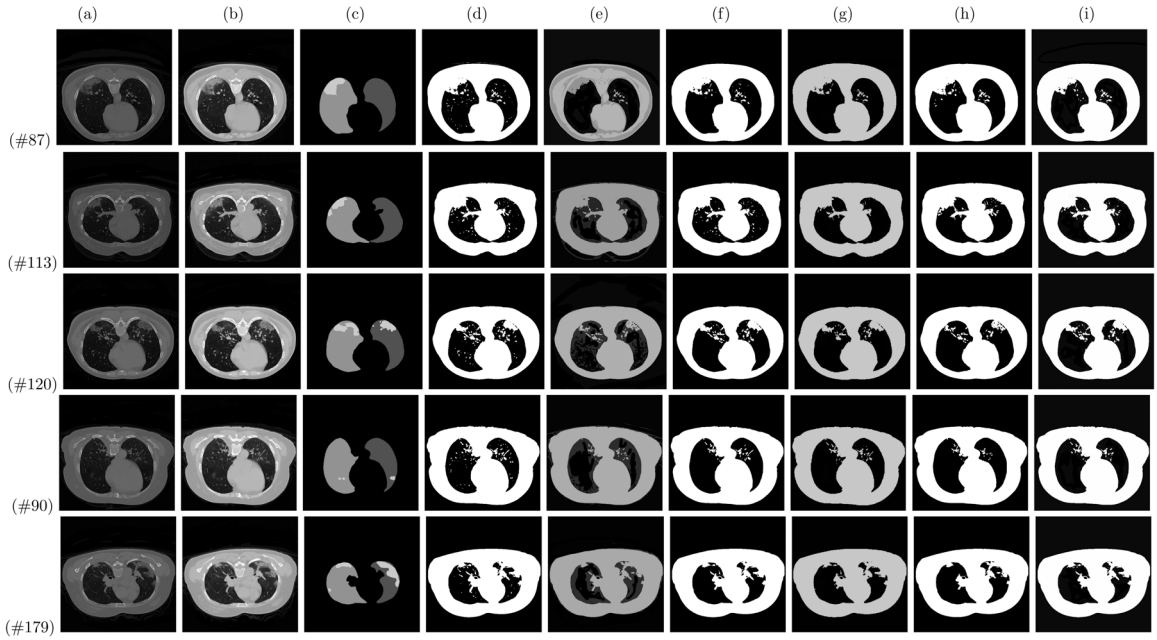

Fig. 7. Segmentation of CT scan images of Experimental_Set_2 (Case labels: 6–10) of COVID-19 using the proposed FFQOAK and existing methods: (a) extracted CT scan image, (b) enhanced CT scan image of (a), (c) GT of (a), (d) proposed FFQOAK, (e) KMC, (f) GAK, (g) PSOK, (h) DPSOK, and (i) ACOK.

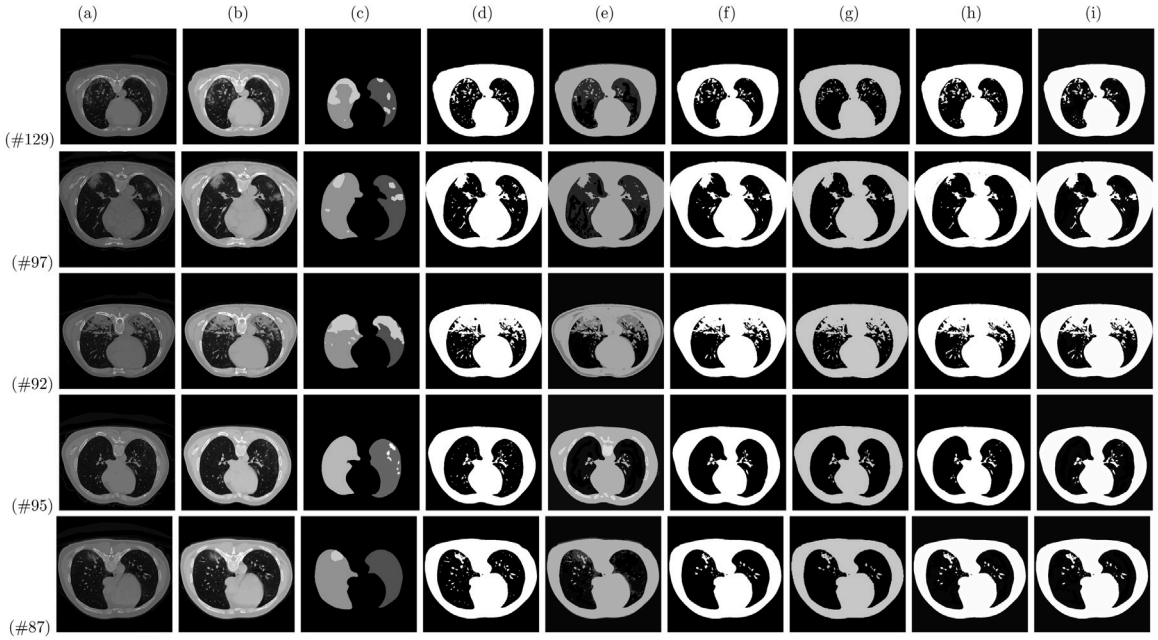

Fig. 8. Segmentation of CT scan images of Experimental_Set_3 (Case labels: 1–5) of COVID-19 using the proposed FFQOAK and existing methods: (a) extracted CT scan image, (b) enhanced CT scan image of (a), (c) GT of (a), (d) proposed FFQOAK, (e) KMC, (f) GAK, (g) PSOK, (h) DPSOK, and (i) ACOK.

the personal best and the global best displacements achieved by the quantum in the quantum system.

This study has proposed a new image segmentation method, called FFQOAK based on FFQOA and KMC algorithm. Considering the prevalence of COVID-19, the proposed FFQOAK method has been employed in segmenting the chest CT scan images of COVID-19 patients (Jun et al., 2020). The aim of this application is to segment these images into different regions and detect the infected regions. In this method, KMC algorithm is used to cluster the gray level values of chest CT scan images. The main strategy of this algorithm is to cluster the gray level values in such a way that the Euclidean distance between the gray level values belonging to each cluster is minimized. In this algorithm, each cluster center is represented by the intensity of the gray level values. However, the KMC algorithm tries to find the best cluster centers for the gray level values with each iteration. Since, the KMC algorithm endures with the problems of optimal cluster centers and global optimum, the FFQOA is used to solve these problems by minimizing the Euclidean distance function. Experimental results show that the FFQOAK method is able to generate optimal segmented images by highlighting the

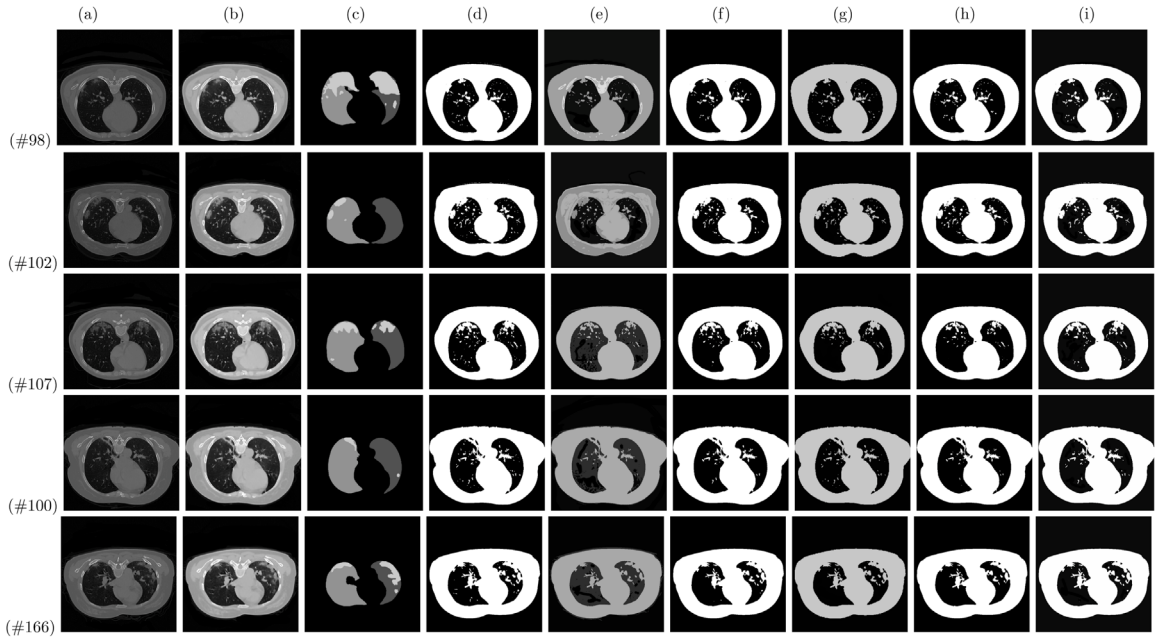

Fig. 9. Segmentation of CT scan images of Experimental_Set_3 (Case labels: 6–10) of COVID-19 using the proposed FFQOAK and existing methods: (a) extracted CT scan image, (b) enhanced CT scan image of (a), (c) GT of (a), (d) proposed FFQOAK, (e) KMC, (f) GAK, (g) PSOK, (h) DPSOK, and (i) ACOK.

Fig. 10. Segmentation of CT scan images of Experimental_Set_4 (Case labels: 1–5) of COVID-19 using the proposed FFQOAK and existing methods: (a) extracted CT scan image, (b) enhanced CT scan image of (a), (c) GT of (a), (d) proposed FFQOAK, (e) KMC, (f) GAK, (g) PSOK, (h) DPSOK, and (i) ACOK.

infected regions with good visual effects in the CT scan images. The performance of the proposed FFQOAK method has been compared with five other methods, including KMC (Juang & Wu, 2010), GAK (Khrissi et al., 2020), PSOK (van der Merwe & Engelbrecht, 2003), DPSOK (Li et al., 2015) and ACOK (Saatchi & Hung, 2005). Various comparative metrics based on mean squared error (MSE), peak signal-to-noise ratio (PSNR), Jaccard similarity coefficient (JSC) and correlation coefficient (CC) show the efficiency of the proposed FFQOAK method.

The remainder of this article is arranged as follows. Section 2 presents the application of the KMC algorithm for image segmentation. The proposed FFQOA is presented in Section 3. The proposed FFQOAK method is presented in Section 4. Experimental results are discussed in Section 5. Finally, conclusions and future directions are presented in Section 6.

2. Image segmentation using KMC algorithm

For an input image I_p, each gray level value $P_i(i = 1, 2, \ldots, n)$ can be defined with n-dimensional vectors, which take their values in the range $[0, G]$ with $G = 255$. That is, for the I_p, the 256 gray levels belong to the universe of discourse $U = [0, G]$. Therefore, a gray level domain (GLD) (Jourlin, 2016) can be described on a set of domains P_i forming a space in the plane U. The GLD is denoted as G_{ld}, and can be expressed

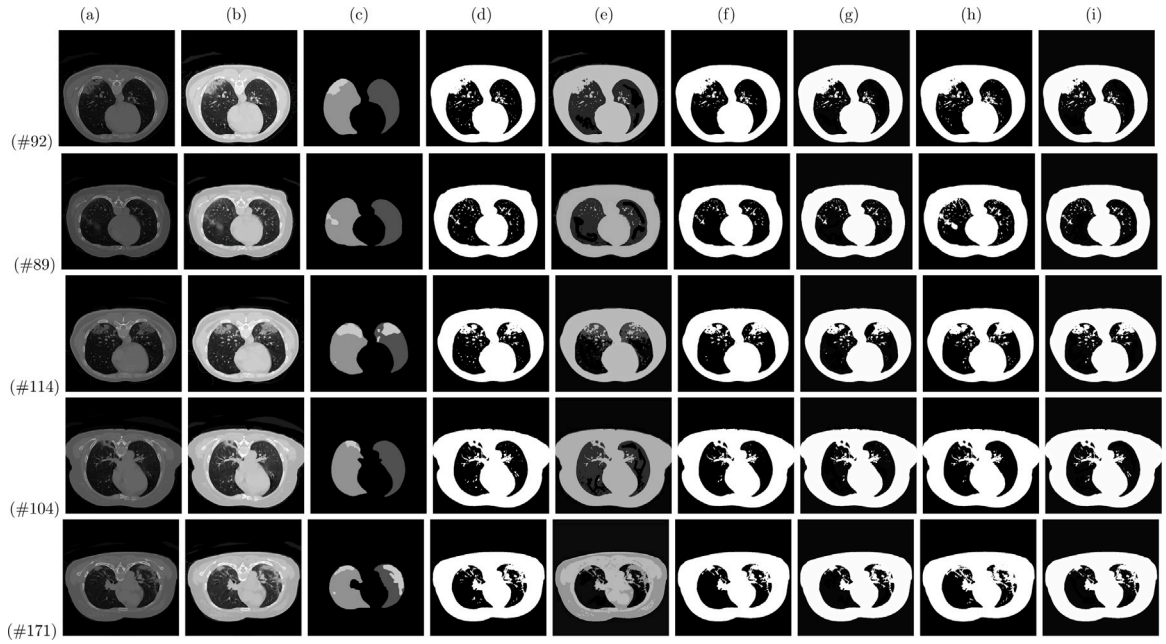

Fig. 11. Segmentation of CT scan images of Experimental_Set_4 (Case labels: 6–10) of COVID-19 using the proposed FFQOAK and existing methods: (a) extracted CT scan image, (b) enhanced CT scan image of (a), (c) GT of (a), (d) proposed FFQOAK, (e) KMC, (f) GAK, (g) PSOK, (h) DPSOK, and (i) ACOK.

as:

$$G_{ld} : P_i \subset \mathbb{R}^2 \rightarrow U \subset \mathbb{R} \tag{2}$$

In the context of clustering G_{ld}, this study uses the KMC algorithm. Steps involved in this algorithm are explained next.

Step 1. **Input:** an image I_p.

Step 2. A set of gray level values $G_{ld} = \{P_1, P_2, \ldots, P_n\}$.

Step 3. Initialize θ number of clusters $z = 1, 2, \ldots, \theta$.

Step 4. Assume a set of randomly initialized cluster centers as $C(e) = \left[C_1(e), C_2(e), \ldots, C_\theta(e)\right]$; where, e represents the 1st epoch of the algorithm.

Step 5. Repeat.

(a) Calculate the Euclidean distance $d[P_i, C_j(e)]$ between gray level value $P_i \in G_{ld}$ and the cluster center $C_j(e) \in C(e)$ using the relation given below as:

$$d[P_i, C_j(e)] = |P_i - C_j(e)|^2 \tag{3}$$

If $C_j(e)$ is the nearest center for the P_i, then it is assigned to the cluster Z_j.

(b) Assign all the gray level values to the closest cluster center based on the minimum Euclidean distance.

(c) Recalculate the new cluster centers using the following equation as:

$$C_j(e+1) = \frac{1}{\eta} \sum_{i=1}^{\eta} P_i; \ (j = 1, 2, \ldots, \theta) \tag{4}$$

Here, η represents the size of the cluster Z_j.

Step 6. Go to **Step 5**, and step up the epoch. This process is continued until the cluster centers stop changing or the algorithm reaches the maximum number of epochs E, i.e., $e = 1, 2, \ldots, E$.

Step 7. **Output:** reshape the θ number of clustered gray level values into a segmented image I_s.

3. The proposed FFQOA

In this section, inspiration, background, mathematical modeling are presented along with the pseudocode of the proposed FFQOA.

3.1. Inspiration for the FFQOA

It is known from experiments that quantum motion is very different from the motion of rigid objects. Since rigid objects consist of many atoms, quantum effects in rigid objects are somehow considered to be averaged. Rigid objects in quantum physics are composed of many quanta, and is called *quantum system* (Fig. 1). In a quantum system, the motion of a microscopic quantum *usually* can be defined by classical mechanics (Levi, 2012). In this approach, the location, movement and displacement of the quantum can be defined in the direction of motion. In this study, it has been assumed that there is an inertial time reference with respect to which a quantum can move to achieve the best displacement. In the quantum system, the search for the best displacement continues until each quantum achieves its own best displacement. Based on this motivation, a new optimization algorithm inspired by the displacement of quantum is proposed in this study. The proposed algorithm is referred to as FFQOA.

3.2. Background for the FFQOA

The FFQOA is a quantum-based heuristic search algorithm based on the simulation of quantum displacement activity within a quantum system. The original goal of the FFQOA is to mathematically simulate the elegant and uncertain displacements of quanta by discovering their patterns that excite the quanta to move by following the Schrödinger equation (Schrödinger, 1935). In the intermediate phase, this algorithm enhances the search scope of the instantaneous movement of individual quantum by rearranging them within the quantum system. Their movements lead to displacements that give both stability and optimal structure to the quantum system. For this purpose, the FFQOA has been developed, which is very simple and effective in solving optimization problems.

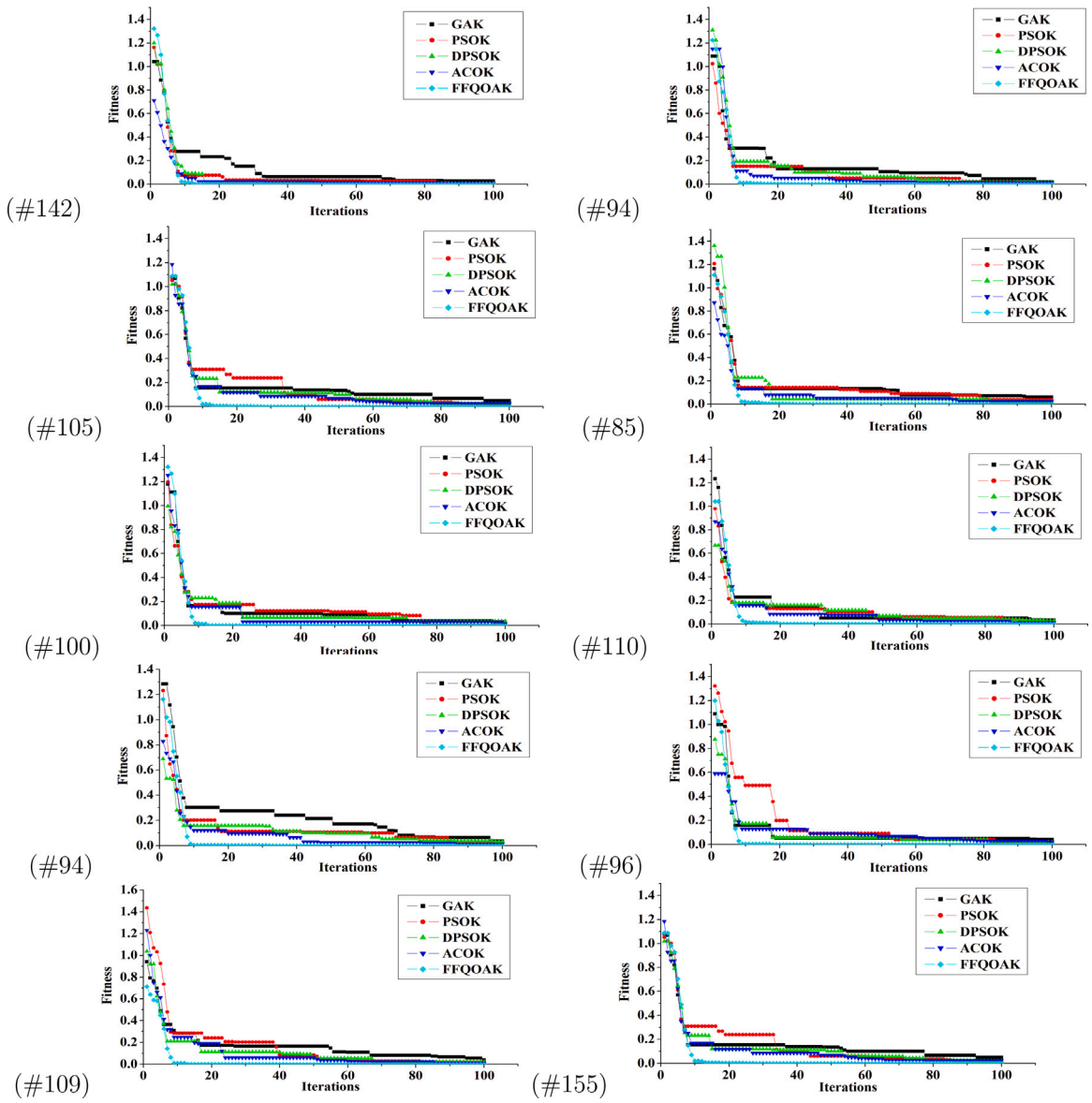

Fig. 12. Convergence curve analysis of Experimental_Set_1 (Case label: 1-10).

In FFQOA, the search agent is called "quantum", which is allowed to move in the multidimensional search space. A collective form of quantum is called *quanta*. Each quantum has its own point of origin, which is called *location*, and the state of change of its location is called *movement*. Movement of quantum leads to change in location, which is called *displacement*. Enhancements in the displacements of quanta are made on the basis of the exchange of information with a successful quantum. A successful quantum is evaluated by the effective displacement. Therefore, the displacement of a quantum is affected by the effective displacement of its surrounding quanta. Consequently, the search activity of a quantum is influenced by other quanta within the quantum system. The result of modeling this interaction operation is that each quantum in the search space shifts in the direction of the preceding quanta. Therefore, each quantum maintains this information in the quantum system: (a) personal location, (b) personal movement, (c) personal displacement, (d) personal successes in the form of displacements, and (e) surrounding successes in the form of displacements. Finally, each quantum attempts to achieve stability in the multidimensional search space by mimicking personal successes and surrounding success.

3.3. Mathematical modeling for the FFQOA

In the following, we provide the mechanism of FFQOA by formulating an optimization problem as:

$$\text{Optimize (Max. or Min.) } f_h(x), (h = 1, 2, \ldots, H), x \in \mathbb{Q} \tag{5}$$

subject to the linear constraints

$$\lambda_j(x) \geq 0, \quad (j = 1, 2, \ldots, J), \tag{6}$$

$$\Theta_m(x) \geq 0, \quad (m = 1, 2, \ldots, M), \tag{7}$$

where, $f_h(x)$, $\lambda_j(x)$ and $\Theta_m(x)$ are functions of the following design vector:

$$x = (x_n), \quad (n = 1, 2, \ldots, N) \tag{8}$$

where, the components x_n of x are called *decision variables*, and N is the number of decision variables. In Eq. (5), the functions $f_h(x)$ are

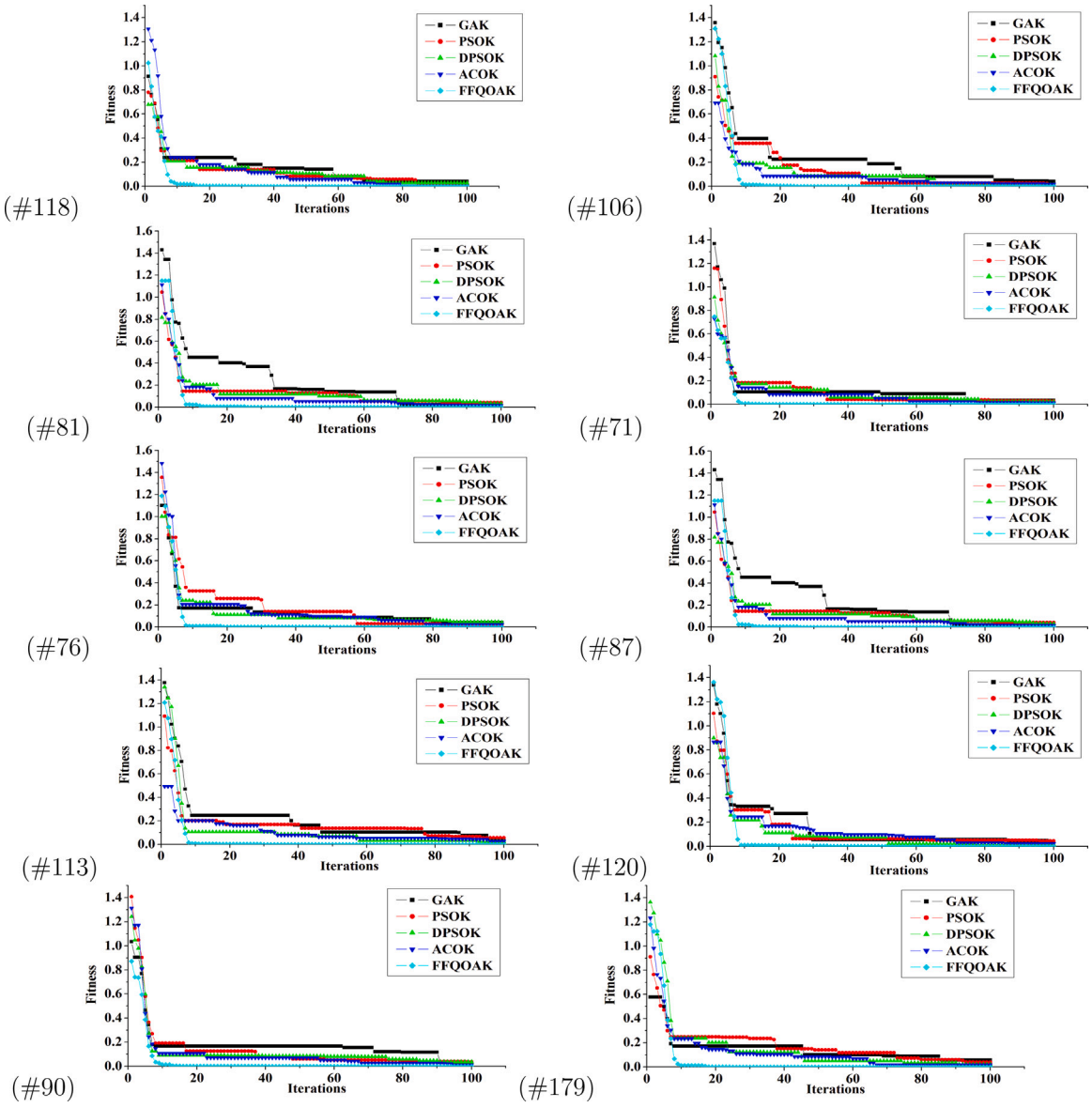

Fig. 13. Convergence curve analysis of Experimental_Set_2 (Case label: 1-10).

referred as the *objective functions*, where $H = 1$ indicates that it is only a single objective. The space expanded by the x_i is called the *quantum system* $\mathbb{Q}$, whereas the space produced by the $f_h(x)$ values is called the *solution space*. In Eqs. (6) and (7), λ_j and Θ_m are called constraints. For these constraints, a condition set is defined for each decision variable x_n as $G^{LB} \leq x_n \leq G^{UB}$, which restricts the value of an x_n within a lower bound (G^{LB}) and an upper bound (G^{UB}).

Step 1. Initialization of quantum in the quantum system: First, assume that the solutions to the optimization problems are scattered in the quantum system. Each quantum is allowed to move to search the solution in this system. A quantum system is defined by initializing each quantum in the search space with the following Schrödinger equation (Schrödinger, 1935) as:

$$Q_k(e) = \phi \cdot Q1_k(e) + (1 - \phi) \cdot Q2_k(e) \tag{9}$$

In Eq. (9), $Q_k(e)$ represents the kth quantum with an epoch e, and $k = 1, 2, \ldots, q$; where q denotes the total number of quanta in the $\mathbb{Q}$. Here, $Q1_k(e)$ and $Q2_k(e)$ are two wave functions for the kth quantum; $\phi = a + ib$ is a complex number, a and b are real numbers in $[0, 1]$ and i is the imaginary unit $i = \sqrt{-1}$. In the representation of complex number, multiplication by -1 refers to a 180-degree rotation about the origin of the kth quantum. Hence, the multiplication by i refers to a 90-degree rotation of the kth quantum in the "positive", counterclockwise direction (Berezin & Shubin, 1991). Since it is not possible to use the complex number ϕ directly to initialize the quantum in the search space, therefore, its absolute value is used in the computation process, defined as $|\phi| = \sqrt{a^2 + b^2}$. Both $Q1_k(e)$ and $Q2_k(e)$ can be defined as:

$$Q1_k(e) = \left\{G^{UB} + r_1 \cdot (G^{UB} - G^{LB})\right\} \tag{10}$$

$$Q2_k(e) = \left\{G^{LB} + r_2 \cdot (G^{UB} - G^{LB})\right\} \tag{11}$$

In Eqs. (10) and (11), r_1 and r_2 represent two different random functions, which are defined in $[0, 1]$, respectively.

Step 2. Location of quantum: To model this, it is assumed that for each quantum there must be a location in the quantum system.

Mathematically, the location acquired by $Q_k(e)$ is denoted as $L_k(e)$, and can be defined as:

$$L_k(e) = \frac{1}{Q_k(e)} e^{-2/Q_k(e)} \tag{12}$$

Step 3. Movement of quantum: To search the solution, each quantum is allowed to move in the quantum system. Mathematically, movement exhibited by $Q_k(e)$ is called $M_k(e)$, and can be defined as:

$$M_k(e) = |Q_k(e) - \frac{L_k(e)}{2} \ln(1/m_f)| \tag{13}$$

Here, m_f is called the *quantum movement factor*, which can be taken in $]0, 1]$.

Step 4. Displacement of quantum: The movement of each quantum provides a displacement to it. The displacement accompanied by each quantum in the quantum system can be defined by the $L_k(e)$ and $M_k(e)$. The displacement of the $Q_k(e)$ is denoted by $D_k(e)$, and can be expressed as:

$$D_k(e) = 2 \cdot |L_k(e) - M_k(e)| \tag{14}$$

Step 5. Fitness evaluation of displacement: A fitness value is determined for $D_k(e)$, and it is updated if a better solution than the previous one exists.

Algorithm 1 PROCEDURE pBD().

```
Define ℚ with q number of quanta: Q_k(e)(k = 1, 2, ..., q) ∈ ℚ (Eq. (9)).
while e < E do
    for ∀Q_k(e) do
        /*get the personal best displacement*/
        if Ĵ(D_i(e)) < Ĵ(D_j(e)) then
            D_j(e) = D_i(e);
        end
        /*get the surrounding best displacement*/
        if Ĵ(D_j(e)) < Ĵ(pBD_k(e)) then
            pBD_k(e) = D_j(e);
        end
    end
    for ∀Q_k(e) do
        Update M_k(e): M_k(e + 1) (Eq. (15)).
        Update D_k(e): D_k(e + 1) (Eq. (20)).
    end
    /*Repeat the process until stopping criterion is satisfied*/
    e = e + 1;
end
```

Step 6. Enhancement of search scope of quantum: Every quantum enhances its search scope by adjusting its corresponding $M_k(e)$. This enhancement of $M_k(e)$ for the next epoch e+1 is represented by $M_k(e+1)$, and can be defined as:

$$M_k(e+1) = M_1 + M_2 + M_3 \tag{15}$$

In Eq. (15), M_1, M_2 and M_3 can defined using the following Eqs. (16)–(18), respectively:

$$M_1 = \alpha \cdot M_k(e) \tag{16}$$

$$M_2 = \ln(1/m_f) \cdot r_3 \cdot [pBD_k(e) - D_k(e)] \tag{17}$$

$$M_3 = \ln(1/m_f) \cdot r_4 \cdot [gBD(e) - D_k(e)] \tag{18}$$

In Eq. (16), α is called the *quantum acceleration factor*, which can be defined as:

$$\alpha = \alpha_{max} - e \times \frac{|\alpha_{max} - \alpha_{min}|}{E} \tag{19}$$

Here, $e = 1, 2, \ldots, E$, where E denotes the maximum number of epochs set for the algorithm. Here, α_{min} and α_{max} can be taken in $[0.1, 0.9]$, where $\alpha_{max} > \alpha_{min}$. In Eq. (17), $pBD_k(e)$ is the *personal best displacement* achieved since the first epoch for the kth quantum. In Eq. (18), the $gBD(e)$ is the *global best displacement* achieved so far among the displacements. In Eqs. (17) and (18), r_3 and r_4 represent two different random functions, which are defined in $[0, 1]$, respectively.

Step 7. Update the displacement of quantum: Every quantum updates its displacement with the help of previous displacement $D_k(e)$ and enhanced search scope $M_k(e+1)$. This adjustment of $D_k(e)$ for the next epoch is represented by $D_k(e+1)$, and can be defined as:

$$D_k(e+1) = D_k(e) + M_k(e+1) \tag{20}$$

3.4. Personal best and global best displacements

The personal best displacement, i.e., $pBD_k(e)$ is the best displacement experienced by the quantum since the first epoch e. By considering the optimization problem (Eq. (5)), the personal best displacement for Eq. (17) at the next epoch $e+1$ is determined as:

$$pBD_k(e+1) = \begin{cases} pBD_k(e); & \text{if } \hat{J}(D_k(e+1)) \geq \hat{J}(pBD_k(e)) \\ D_k(e+1); & \text{if } \hat{J}(D_k(e+1)) < \hat{J}(pBD_k(e)) \end{cases} \tag{21}$$

Here, $\hat{J}$ denotes the fitness function, which calculates how the corresponding displacement is close to the optimal solution.

For the global best displacement, surrounding quanta act like a network within the quantum system. For the enhancement of search scope, this network is used to extract information from all the quanta. In this case, network information is the best displacement among the quanta, denoted as the $gBD(e)$ for the epoch e. For Eq. (18), it can be obtained as:

$$gBD(e) \in \{pBD_1(e), pBD_2(e), \ldots, pBD_q(e)\} \mid \hat{J}(gBD(e)) = \min\{pBD_1(e), pBD_2(e), \ldots, pBD_q(e)\} \tag{22}$$

Determination procedures for the personal best and global best displacements are summarized in Algorithm 1 and Algorithm 2, respectively.

Algorithm 2 PROCEDURE gBD().

```
Define ℚ with q number of quanta: Q_k(e)(k = 1, 2, ..., q) ∈ ℚ (Eq. (9)).
while e < E do
    for ∀Q_k(e) do
        /*get the personal best displacement*/
        if Ĵ(D_i(e)) < Ĵ(D_j(e)) then
            D_j(e) = D_i(e);
        end
        /*get the global best displacement*/
        if Ĵ(D_j(e)) < Ĵ(gBD(e)) then
            gBD(e) = D_j(e);
        end
    end
    for ∀Q_k(e) do
        Update M_k(e): M_k(e + 1) (Eq. (15)).
        Update D_k(e): D_k(e + 1) (Eq. (20)).
    end
    /*Repeat the process until stopping criterion is satisfied*/
    e = e + 1;
end
```

3.5. The search scope components

The search scope enhancement equation (Eq. (15)) is comprised of three components as:

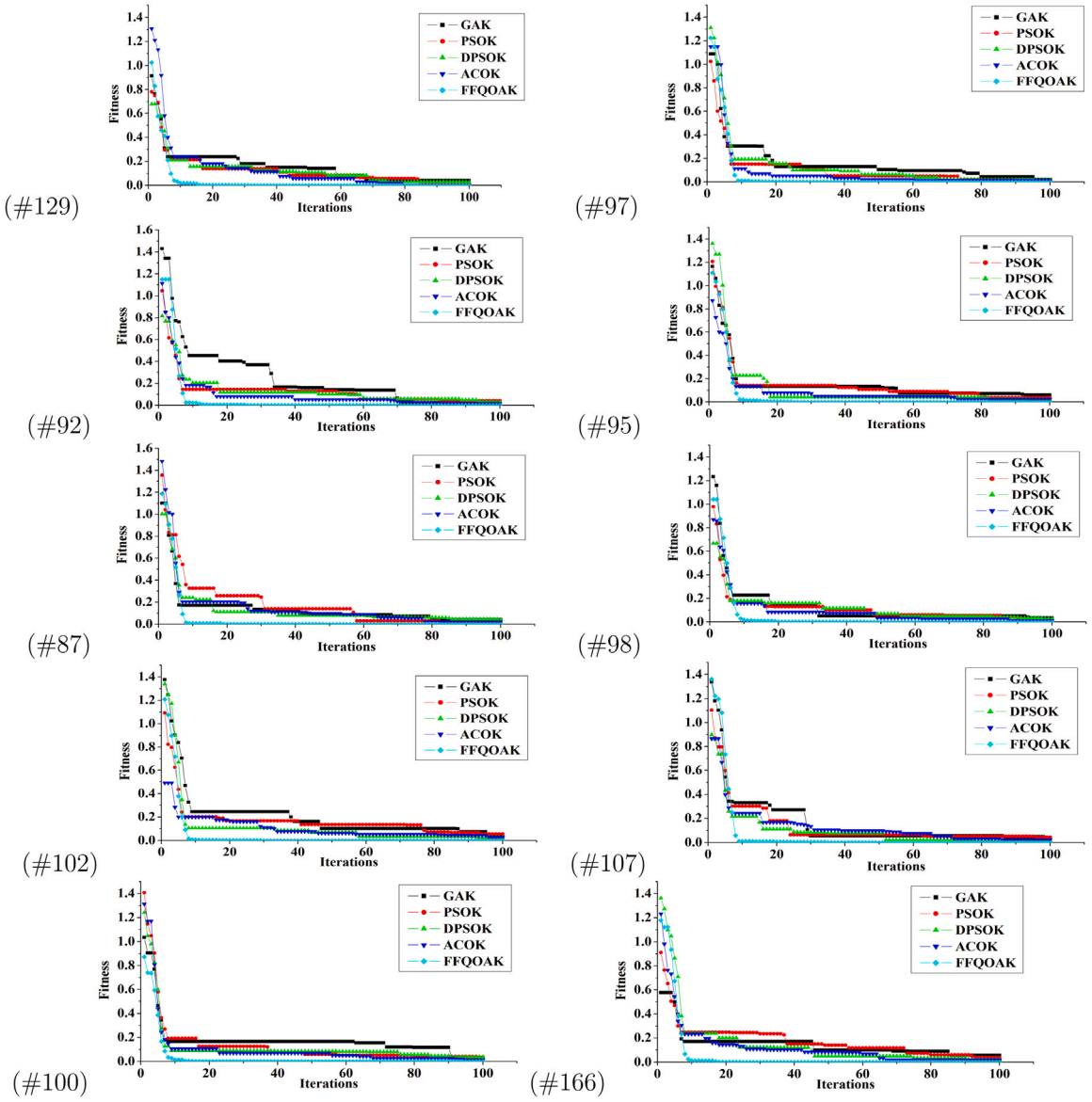

Fig. 14. Convergence curve analysis of Experimental_Set_3 (Case label: 1-10).

- In M_1 (Eq. (16)), the $M_k(e)$ term stores information about the preceding movement information, i.e., information about the prior immediate movement path. The integration of α with $M_k(e)$, i.e., "$\alpha \cdot M_k(e)$" term can be viewed as an accelerated component that prevents the quantum from radically altering movement and influencing towards the present movement. Hence, this component is termed as the *preceding movement component* of the quantum.
- In M_2 (Eq. (17)), the "$\ln(1/m_f) \cdot r_3 \cdot [pBD_k(e) - D_k(e)]$" term maintains the personal network information of the $Q_k(e)$ in terms of past displacements. In a context, this component embodies individual knowledge of the displacement, which was the best for the quantum at the personal network level. The procedure for computing the personal best displacement in this network level is presented as Algorithm 1. The advantage of this component is that it attracts quanta towards their own personal best displacements. This activity resembles the quanta's propensity to attain those displacements that have provided stability to them most during their past displacements. This component is referred to the *personal network component* of the quantum.
- In M_3 (Eq. (18)), the "$\ln(1/m_f) \cdot r_4 \cdot [gBD(e) - D_k(e)]$" term maintains the global network information of the $Q_k(e)$ by quantifying the fitness of the kth quantum with respect to surrounding quanta. This component's effect is that each quantum is attracted to the global best displacement discovered by the quantum's surrounding. The procedure for computing the global best displacement in this network level is presented as Algorithm 2. This component is termed as the *global network component* of the quantum.

A vector representation of the search scope enhancement equation (Eq. (15)) can naively be represented in a two-dimensional search space. For the ease of interpretation, a quantum can be assumed in a two-dimensional search space. An example of the search scope enhancement of the quantum is depicted in Fig. 2. Fig. 2(a) indicates the stage of $D_k(e)$ for the $Q_k(e)$ at the epoch e. It should be noted that the $D_k(e)$ makes the $Q_k(e)$ closer to the $pBD_k(e)$. For the epoch $e+1$, the process of search scope enhancement is updated, which is shown in

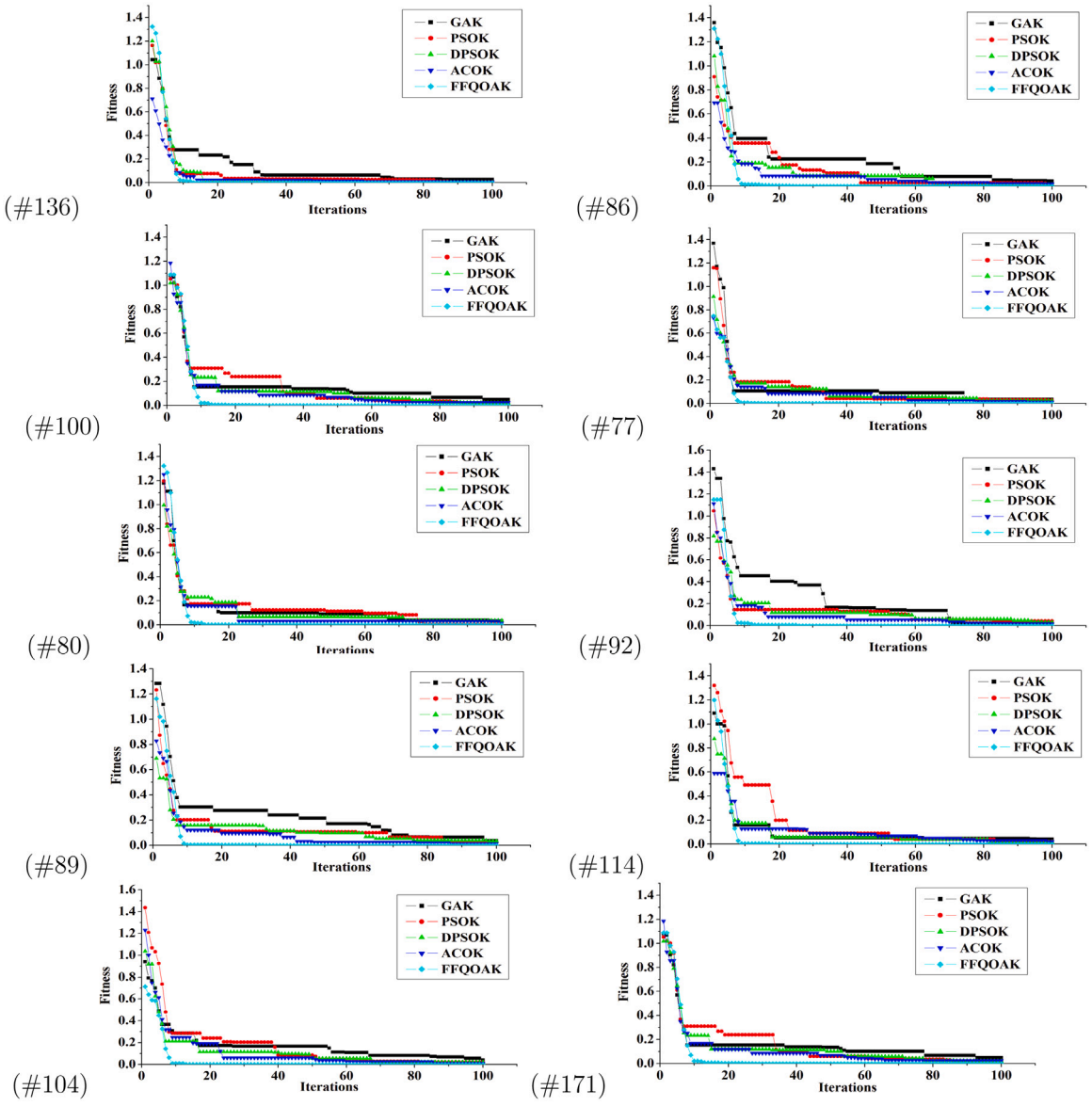

Fig. 15. Convergence curve analysis of Experimental_Set_4 (Case label: 1-10).

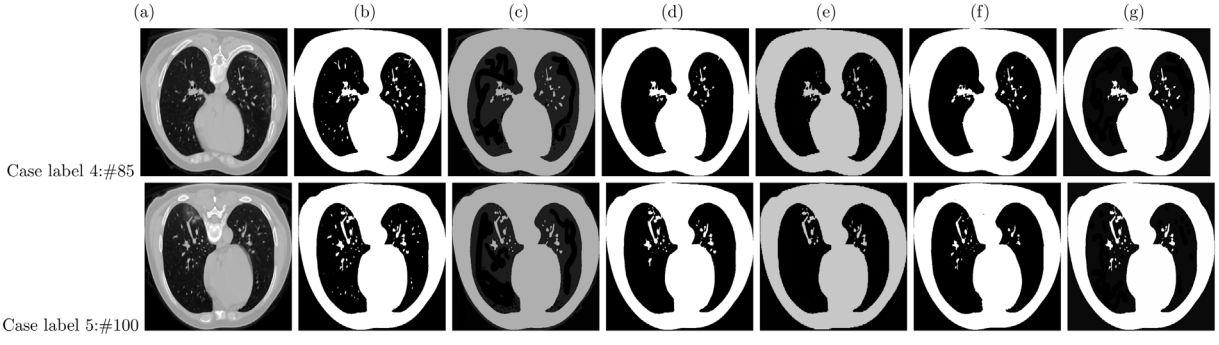

Fig. 16. Visual analysis of segmented results of Experimental_Set_1 (Case labels: 4 and 5): (a) enhanced and enlarged CT scan image, (b) proposed FFQOAK, (c) KMC, (d) GAK, (e) PSOK, (f) DPSOK, and (g) ACOK.

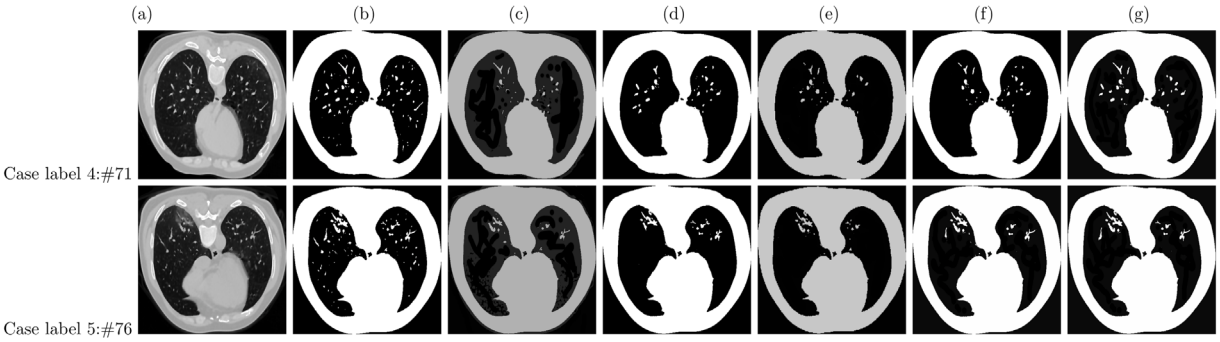

Fig. 17. Visual analysis of segmented results of Experimental_Set_2 (Case labels: 4 and 5): (a) enhanced and enlarged CT scan image, (b) proposed FFQOAK, (c) KMC, (d) GAK, (e) PSOK, (f) DPSOK, and (g) ACOK.

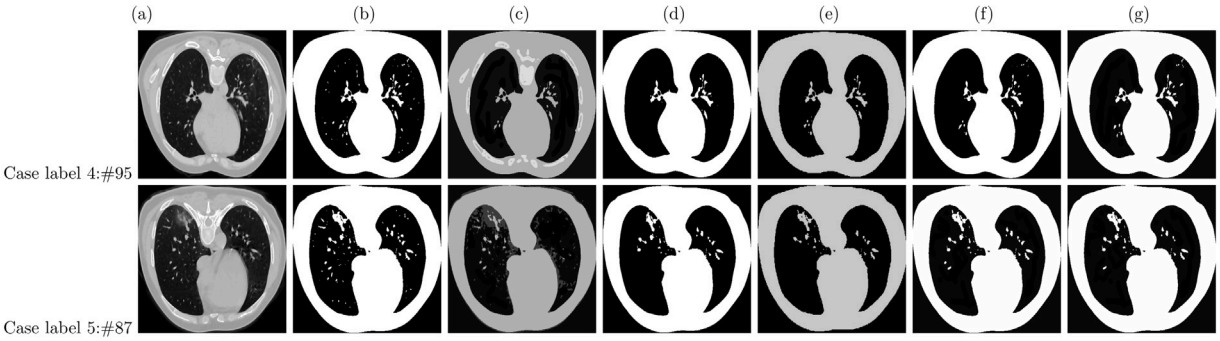

Fig. 18. Visual analysis of segmented results of Experimental_Set_3 (Case labels: 4 and 5): (a) enhanced and enlarged CT scan image, (b) proposed FFQOAK, (c) KMC, (d) GAK, (e) PSOK, (f) DPSOK, and (g) ACOK.

Fig. 2(b). The figure shows that the $D_k(e+1)$ contributes to the quantum by taking it closer to the $gBD(e+1)$.

The proposed FFQOA is summarized in Algorithm 3 in terms of q number of quanta in the $\mathbb{Q}$.

Algorithm 3 PROCEDURE FFQOA().

Define $\mathbb{Q}$ with q number of quanta: $Q_k(e)(k = 1, 2, \ldots, q) \in \mathbb{Q}$ (Eq. (9)).
for $\forall Q_k(e)$ **do**
  Define location of each quantum: $L_k(e)$ (Eq. (12)).
  Define movement of each quantum: $M_k(e)$ (Eq. (13)).
  Compute displacement of each quantum: $D_k(e)$ (Eq. (14)).
  Evaluate the fitness of each displacement $D_k(e)$ to get: $pBD_k(e)$ (Algorithm 1) and $gBD(e)$ (Algorithm 2).
end
while $e < E$ **do**
  for *each* $Q_k(e)$ **do**
    Update $M_k(e)$: $M_k(e+1)$ (Eq. (15)).
    Update $D_k(e)$: $D_k(e+1)$ (Eq. (20)).
  end
  /*Repeat the process until stopping criterion is satisfied*/
  e=e+1;
end

4. The proposed FFQOAK method

This section introduces the proposed FFQOAK method along with its searching processes of optimal solution.

4.1. Phases of the FFQOAK method

Each phase of the proposed method is explained next.

Step 1. **Input:** an image I_p.

Step 2. A set of gray level values $G_{ld} = \{P_1, P_2, \ldots, P_n\}$.

Step 3. Initialize θ number of clusters $z = 1, 2, \ldots, \theta$.

Step 4. Obtain the set of initial cluster centers as $C = [C_1, C_2, \ldots, C_\theta]$ using KMC algorithm.

Step 5. Apply the FFQOAK in the G_{ld} to get the optimal segmented image I_s as:

sub-step 5.1. **Initialization of quantum in the quantum system:** Analogue to **Step 1** of FFQOA.

sub-step 5.2. **Location of quantum:** Analogue to **Step 2** of FFQOA.

sub-step 5.3. **Movement of quantum:** Analogue to **Step 3** of FFQOA.

sub-step 5.4. **Displacement of quantum:** Obtain the displacement (analogue to **Step 4** of FFQOA), and assign the set of initial cluster centers C to any displacement $D_j(e)$.

sub-step 5.5. Repeat.

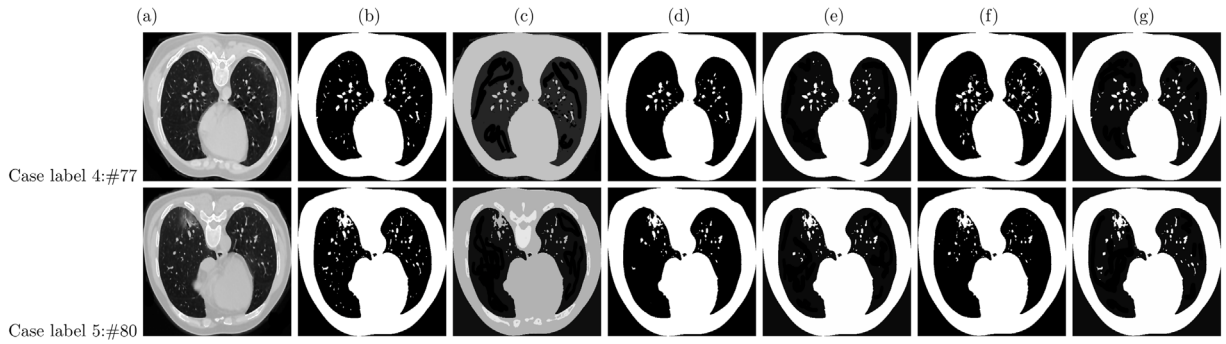

Fig. 19. Visual analysis of segmented results of Experimental_Set_4 (Case labels: 4 and 5): (a) enhanced and enlarged CT scan image, (b) proposed FFQOAK, (c) KMC, (d) GAK, (e) PSOK, (f) DPSOK, and (g) ACOK.

(a) **Calculation of Euclidean distance:** Calculate the Euclidean distance between gray level value $P_i \in G_{ld}$ and the displacement $D_j(e)$ using the relation given below as:

$$d[P_i, X_z] = |P_i - X_z|^2;\ \forall X_z \in D_j(e) \tag{23}$$

If X_z is the nearest center to P_i, then it is assigned to cluster Z_z.

(b) **Assignment of gray level values:** Assign all the gray level values to the closest center based on the minimum Euclidean distance.

(c) **Fitness evaluation of cluster center:** Evaluate the fitness of jth cluster center $D_j(e)$, which can be defined as:

$$\hat{J}_j(e) = \sum_{i=1}^{n} |P_i - X_z|^2 \tag{24}$$

The value of $\hat{J}_j(e)$ is considered to be optimal, when it satisfies the following condition:

$$\frac{\partial \hat{J}_j(e)}{\partial X_z} = \frac{\partial}{\partial X_z} \sum_{i=1}^{n} |P_i - X_z|^2 = -2 \sum_{i=1}^{n} |P_i - X_z| = 0 \tag{25}$$

The average fitness of all displacements in the $\mathbb{Q}$, where $\mathbb{Q} \subseteq D_j(e)$, is computed as:

$$\hat{J}_{avg}(e) = \frac{1}{\theta} \sum_{j=1}^{\theta} \hat{J}_j(e) \tag{26}$$

sub-step 5.6. Enhancement of search scope of quantum: Analogue to **Step 6** of FFQOA.

sub-step 5.7. Update the displacement of quantum: Analogue to **Step 7** of FFQOA.

sub-step 5.8. Go to **sub-step 5.8.**, and step up the epoch. This process is continued until the cluster centers stop changing or the algorithm reaches the maximum number of epochs E, i.e., $e = 1, 2, \ldots, E$.

Step 6. Output: reshape the θ number of clustered gray level values into a segmented image I_s.

Algorithm 4 PROCEDURE FFQOAK().

Input: an image I_p.
A set of gray level values $G_{ld} = \{P_1, P_2, \ldots, P_n\}$.
Initialize θ number of clusters $z = 1, 2, \ldots, \theta$.
Obtain the initial cluster centers: $C = [C_1, C_2, \ldots, C_\theta]$ (using KMC algorithm).
/*Apply the FFQOAK in the G_{ld} to get the optimal segmented image I_s*/
for $\forall Q_k(e)$ **do**
  Define $\mathbb{Q}$ with q number of quanta: $Q_k(e)(k = 1, 2, \ldots, q) \in \mathbb{Q}$ (Eq. (9)).
  Define location of each quantum: $L_k(e)$ (Eq. (12)).
  Define movement of each quantum: $M_k(e)$ (Eq. (13)).
  Obtain the displacement (Eq. (14)), and assign the set of initial cluster centers C to any displacement $D_j(e)$.
end
while $e < E$ **do**
  for $\forall Q_k(e)$ **do**
    Calculate the Euclidean distance between gray level value $P_i \in G_{ld}$ and the displacement $D_j(e)$ (Eq. (23)).
    Assign all the gray level values to the closest center based on the minimum Euclidean distance.
    Evaluate the fitness of jth cluster center $D_j(e)$ (Eq. (24)) to get: $pBD_k(e)$ (Algorithm 1) and $gBD(e)$ (Algorithm 2).
    Update the $M_k(e)$: $M_k(e+1)$ (Eq. (15)).
    Update the $D_k(e)$: $D_k(e+1)$ (Eq. (20)).
  end
  /*Repeat the process until there is no change in the cluster centers.*/
  e=e+1;
end
Output: reshape the θ number of clustered gray level values into a segmented image I_s.

The proposed FFQOAK method is summarized in Algorithm 4 in terms of q number of quanta in the $\mathbb{Q}$.

4.2. Optimization process of the proposed FFQOAK method

The FFQOAK is comprised of six major stages in the segmentation of images as:

Stage I: For each quantum, a quantum system is defined and its displacement is calculated.

Stage II: The initial displacement of each quantum is considered as the initial cluster center.

Stage III: Each displacement (**Stage II**) is assigned to the Euclidean distance function of the KMC algorithm.

Stage IV: The fitness parameter is used to evaluate the fitness of each cluster center

Stage V: The search scope of each quantum is enhanced by updating its movement and displacement within the quantum system.

Stage VI: Go to **Stage III** with updated displacements, until it discovers the optimal global solution or the nearest optimal global solution.

The FFQOAK is implemented in Matlab R2014a version (8.3.0.532) in Microsoft Windows 8.1 environment on Core i-5 processor with 3.20 GHz and 8 GB memory. Based on Singh (2021a), various parameters associated with the proposed FFQOAK are set as:

- Number of clusters, $\theta = 3$,
- Number of quanta, $Q = 20$,
- Real numbers, $a = 0.1$ and $b = 0.1$,
- Quantum movement factor, $m_f = 0.14$,
- $\alpha_{max} = 0.9$, $\alpha_{min} = 0.2$, and
- Maximum number of epochs, $E = 100$.

Each image has been preprocessed before segmentation due to noise and low contrast features. This is done using the adaptive filtering technique (Douglas & Losada, 2002), followed by the histogram equalization method (Han, Yang, & Lee, 2011). The preprocessed image is called *enhanced CT scan image*. Some of the essential processes of the proposed FFQOAK are illustrated by a chest CT scan image of COVID-19 in Fig. 3. The input and its enhanced CT scan images are shown in Fig. 3(a) and (b), respectively. The proposed FFQOAK is applied to the enhanced CT scan image for segmentation. The search landscape of the fitness evaluation metric is shown in Fig. 3(c). Comparison of fitness values between the first quantum and the optimal quantum is shown in Fig. 3(d). Their differences show that the optimal quantum converges very well by avoiding the local optimal solution. The convergence curve of the average fitness values is shown in Fig. 3(e), and shows that all quanta perform well in finding the optimal solution at each epoch. But, only a certain quantum reaches the global optimal solution. The search history curve, as shown in Fig. 3(f), demonstrates the location history of the quanta during the search for the global optimal solution. Using the optimal cluster centers, the input image is reshaped to form the segmented image. This segmented image is shown in Fig. 3(g).

It can be observed that by including FFQOA, FFQOAK can achieve fast convergence. The initial cluster centers optimized in **Stage III** can be considered as the global optimal cluster centers of the KMC algorithm. Therefore, the requirement of adopting the initial cluster centers for the KMC algorithm in the next stages no longer exists.

5. Experimental results

This section includes descriptions of the dataset and its preprocessing, performance evaluation metrics, statistical analyses, convergence analysis and finally visual analysis.

5.1. Dataset and preprocessing descriptions

The proposed FFQOAK method has been evaluated with different types of chest CT scan images of COVID-19 patients obtained from Jun et al. (2020). This dataset contains 20 labeled COVID-19 CT scan images. For experimental purposes, 10 labeled COVID-19 CT scan images are used, which are labeled as Case 1, Case 2, and so on. From each label, four different images are extracted and arranged in four experimental sets, namely Experimental_Set_1, Experimental_Set_2, Experimental_Set_3 and Experimental_Set_4. Each experimental set contains ground truth (GT) of the respective image. The descriptions of the features associated with each experimental set in terms of case label, extracted images, original image size (in kB) and enhanced image size (in kB) are listed in Table 1. The main objective of splitting the dataset into four sets is to evaluate whether the same set of parameters of FFQOAK used for the Experimental_Set_1 is suitable for the other experimental sets or not.

Table 1
Features of selected images of chest CT scan images of COVID-19.

Dataset	Case label	Extracted image	Extracted CT scan image size (in kB)	Enhanced CT scan image size (in kB)
Experimental_Set_1	1	#142	169	129
	2	#94	237	172
	3	#105	218	154
	4	#85	202	146
	5	#100	207	155
	6	#110	211	140
	7	#94	212	134
	8	#96	184	126
	9	#109	181	130
	10	#155	173	121
Experimental_Set_2	1	#118	179	120
	2	#106	231	7.15
	3	#81	216	152
	4	#71	191	144
	5	#76	193	147
	6	#87	211	150
	7	#113	225	149
	8	#120	169	127
	9	#90	173	136
	10	#179	177	130
Experimental_Set_3	1	#129	188	124
	2	#97	250	164
	3	#92	223	150
	4	#95	206	139
	5	#87	210	143
	6	#98	222	141
	7	#102	222	139
	8	#107	192	129
	9	#100	185	137
	10	#166	179	127
Experimental_Set_4	1	#136	173	71.0
	2	#86	223	92.5
	3	#100	190	81.6
	4	#77	179	82.2
	5	#80	179	80.9
	6	#92	191	83.0
	7	#89	177	76.5
	8	#114	181	75.3
	9	#104	185	77.8
	10	#171	163	70.6

5.2. Performance evaluation metrics

The performance of the proposed FFQOAK method has been evaluated by comparing the segmented slices with GT. For this purpose, well-known statistical metrics are used, namely MSE, PSNR, JSC and CC. Such metrics can evaluate the performance of the proposed FFQOAK in terms of its consistency with the GT. These metrics are defined in terms of the input image (I_p), the segmented image (I_s) and the respective GT (I_g) as (Huang, Singh and Kuo, 2020):

- **MSE:** The MSE value is used to measure an average loss in intensity of gray level values during the segmentation of I_p. A smaller MSE value implies less intensity loss and results in better I_s. Mathematically, this can be expressed as:

$$MSE = \frac{1}{U \times V} \sum_{u=1}^{U} \sum_{v=1}^{V} (I_p - I_s)^2 \tag{27}$$

Here, $U \times V$ represents the size of image in terms of pixels.

Table 2
Comparison of MSE with the existing methods and the proposed FFQOAK for the chest CT scan images of COVID-19.

Dataset	Case label	Extracted image	KMC	GAK	PSOK	DPSOK	ACOK	FFQOAK
Experimental_Set_1	1	#142	7106.24	2101.60	1579.67	1419.67	1119.34	**719.12**
	2	#94	6140.72	2108.73	1800.24	1700.14	1010.15	**810.21**
	3	#105	4465.27	2192.48	1218.01	1113.01	1013.01	**713.32**
	4	#85	6294.26	2191.21	1265.11	1065.11	1065.11	**615.45**
	5	#100	6310.28	2191.91	1214.44	1114.10	1014.23	**614.12**
	6	#110	4976.81	2110.35	1786.87	1386.23	1086.45	**711.45**
	7	#94	6014.15	2111.36	1848.87	1248.15	1018.12	**718.12**
	8	#96	3219.35	2148.27	2690.30	1290.30	1090.13	**710.11**
	9	#109	5737.93	2191.90	2636.93	1336.93	1036.93	**736.12**
	10	#155	5664.07	2192.73	2844.77	1344.77	1044.77	**714.14**
Experimental_Set_2	1	#118	4798.78	2193.26	1413.13	1113.13	1013.13	**709.12**
	2	#106	5098.64	2192.25	1406.40	1106.40	1006.14	**800.11**
	3	#81	2026.53	2164.63	1231.64	1131.64	1011.64	**703.12**
	4	#71	4830.01	2116.22	1794.11	1294.11	1024.11	**725.15**
	5	#76	5393.30	2117.85	1276.13	1176.13	1016.23	**714.12**
	6	#87	4594.02	2124.75	1156.87	1056.87	1016.27	**716.45**
	7	#113	5739.52	2175.23	1645.72	1245.72	1045.72	**718.12**
	8	#120	8951.75	2127.63	1585.28	1285.28	1085.28	**810.11**
	9	#90	5436.72	2112.82	1132.82	1032.82	1032.82	**716.12**
	10	#179	4594.02	2124.75	1156.87	1056.87	1016.87	**714.14**
Experimental_Set_3	1	#129	6116.24	2111.10	2519.67	1419.17	1219.54	**619.45**
	2	#97	5140.72	2128.13	2810.24	1610.24	1110.15	**640.22**
	3	#92	4365.17	2092.58	1318.11	1213.01	1113.21	**733.32**
	4	#95	6284.16	2161.24	1365.31	1165.11	1265.11	**715.45**
	5	#87	6410.18	2391.95	1312.42	1214.10	1314.23	**614.12**
	6	#98	5976.31	2120.15	1686.57	1376.23	1286.45	**716.45**
	7	#102	5012.15	2131.16	1948.77	1348.15	1118.12	**728.12**
	8	#107	3119.15	2248.17	2590.32	1390.30	1191.13	**717.11**
	9	#100	4737.13	2291.91	2646.83	1346.93	1138.93	**711.12**
	10	#166	4614.17	2292.13	2644.87	1314.75	1244.77	**745.64**
Experimental_Set_4	1	#136	5126.64	2211.20	1219.67	1519.12	1319.14	**729.33**
	2	#86	5210.72	2328.13	1910.14	1620.21	1210.25	**710.12**
	3	#100	5165.17	2192.38	1818.21	1413.21	1213.23	**723.66**
	4	#77	7184.16	2361.14	1765.32	1365.11	1165.21	**625.15**
	5	#80	6310.38	2491.95	1612.45	1314.12	1214.24	**724.22**
	6	#92	5878.36	2320.15	1786.67	1476.43	1486.41	**716.65**
	7	#89	5115.35	2241.66	1848.71	1448.25	1218.22	**768.22**
	8	#114	3219.35	2143.27	2690.31	1491.32	1291.23	**717.11**
	9	#104	4837.23	2491.92	2746.82	1446.82	1238.92	**732.42**
	10	#171	4514.27	2392.23	2844.82	1214.54	1344.17	**715.45**
Average	–	–	5293.23	2203.31	1844.26	1305.61	1136.73	**712.30**

- **PSNR:** The PSNR is inversely related to the MSE, i.e., a higher value shows less distortion and thus a better I_s. Mathematically, this can be expressed as:

$$PSNR = 10 \times \log_{10}\left[\frac{(255)^2}{MSE}\right] \tag{28}$$

- **JSC:** JSC evaluates the similarity between the I_s and I_g. It is defined as the size of the intersection of the pixel sets divided by the size of the union of the pixel sets from the I_s and I_g. The JSC value lies between the range 0–100%. A JSC value near 100% means that the region of interest of the I_s has a perfect similarity to the corresponding I_g. Mathematically, this can be expressed as:

$$J_{I_s,I_g}(X) = \frac{O_{I_s \cap I_g}(X)}{O_{I_s \cup I_g}(X)} \tag{29}$$

In Eq. (29), $O_{I_s \cap I_g}(X)$ and $O_{I_s \cup I_g}(X)$ denote the intersection and union of the pixel sets associated with the X class of I_s and I_g, respectively.

- **CC:** The CC test is used to determine the similarity between I_s and I_g. The range for CC is defined between $[-1, 1]$. A value for CC close to 1 indicates a perfect match between the segmented regions and the respective GT. Mathematically, this can be expressed:

$$r = \frac{\sum_{u=1}^{U}\sum_{v=1}^{V}(I_s - \bar{I}_s)(I_g - \bar{I}_g)}{\left(\sum_{u=1}^{U}\sum_{v=1}^{V}(I_s - \bar{I}_s)^2\right)\left(\sum_{u=1}^{U}\sum_{v=1}^{V}(I_g - \bar{I}_g)^2\right)}; \quad -1 \le r \le 1 \tag{30}$$

where, r indicates the CC value. In Eq. (30), $\bar{I}_s$ and $\bar{I}_g$ represent the means of I_s and I_g, respectively.

5.3. Statistical analyses

In Figs. 4–11(a)~(b), extracted CT scan images and their respective enhanced images of COVID-19 patients are shown in columns. Figs. 4–11(c) show the GT of the respective images of Figs. 4–11(a). Figs. 4–11(d) show segmented images obtained by the proposed FFQOAK method. Segmented images obtained using the existing methods such as KMC (Juang & Wu, 2010), GAK (Khrissi et al., 2020), PSOK (van der Merwe & Engelbrecht, 2003), DPSOK (Li et al., 2015) and ACOK (Saatchi & Hung, 2005) are shown in Figs. 4–11(e)~(i), respectively. These segmented images are obtained with the number of clusters $\theta = 3$. Since all these images are in gray scale, clustering with more than $\theta = 3$ does not produce significant features of infections in the lungs.

Table 3
Comparison of PSNR with the existing methods and the proposed FFQOAK for the chest CT scan images of COVID-19.

Dataset	Case label	Extracted image	KMC	GAK	PSOK	DPSOK	ACOK	FFQOAK
Experimental_Set_1	1	#142	9.61	14.91	16.15	16.61	17.64	**19.56**
	2	#94	10.25	14.89	15.58	15.83	18.09	**19.04**
	3	#105	11.63	14.72	17.27	17.67	18.07	**19.60**
	4	#85	10.14	14.72	17.11	17.86	17.86	**20.24**
	5	#100	10.13	14.72	17.29	17.66	18.07	**20.25**
	6	#110	11.16	14.89	15.61	16.71	17.77	**19.61**
	7	#94	10.34	14.89	15.46	17.17	18.05	**19.57**
	8	#96	13.05	14.81	13.83	17.02	17.76	**19.62**
	9	#109	10.54	14.72	13.92	16.87	17.97	**19.46**
	10	#155	10.60	14.72	13.59	16.84	17.94	**19.59**
Experimental_Set_2	1	#118	11.32	14.72	16.63	17.67	18.07	**19.62**
	2	#106	11.06	14.72	16.65	17.69	18.10	**19.10**
	3	#81	15.06	14.78	17.23	17.59	18.08	**19.66**
	4	#71	11.29	14.88	15.59	17.01	18.03	**19.53**
	5	#76	10.81	14.87	17.07	17.43	18.06	**19.59**
	6	#87	11.51	14.86	17.50	17.89	18.06	**20.25**
	7	#113	10.54	14.76	15.97	17.18	17.94	**19.57**
	8	#120	8.61	14.85	16.13	17.04	17.78	**19.05**
	9	#90	10.78	14.88	17.59	17.99	17.99	**19.58**
	10	#179	11.51	14.86	17.50	17.89	18.06	**19.59**
Experimental_Set_3	1	#129	10.27	14.89	14.12	16.61	17.27	**20.21**
	2	#97	11.02	14.85	13.64	16.06	17.68	**20.07**
	3	#92	11.73	14.92	16.93	17.29	17.67	**19.48**
	4	#95	10.15	14.78	16.78	17.47	17.11	**19.59**
	5	#87	10.06	14.34	16.95	17.29	16.94	**19.59**
	6	#98	10.37	14.87	15.86	16.74	17.04	**19.58**
	7	#102	11.13	14.84	15.23	16.83	17.65	**19.51**
	8	#107	13.19	14.61	14.00	16.70	17.37	**19.57**
	9	#100	11.38	14.53	13.90	16.84	17.57	**19.61**
	10	#166	11.49	14.53	13.91	16.94	17.18	**19.41**
Experimental_Set_4	1	#136	11.03	14.68	17.27	16.31	16.93	**19.50**
	2	#86	10.96	14.46	15.32	16.04	17.30	**19.62**
	3	#100	11.00	14.72	15.53	16.63	17.29	**19.54**
	4	#77	9.57	14.40	15.66	16.78	17.47	**20.17**
	5	#80	10.13	14.17	16.06	16.94	17.29	**19.53**
	6	#92	10.44	14.48	15.61	16.44	16.41	**19.58**
	7	#89	11.04	14.63	15.46	16.52	17.27	**19.28**
	8	#114	13.05	14.82	13.83	16.40	17.02	**19.57**
	9	#104	11.28	14.17	13.74	16.53	17.20	**19.48**
	10	#171	11.58	14.34	13.59	17.29	16.85	**19.59**
Average	–	–	11.02	14.70	15.68	17.01	17.60	**19.61**

Based on the segmented images, it is easy to determine that the infected regions in the extracted images are not sufficiently segmented by the existing methods (Juang & Wu, 2010; Khrissi et al., 2020; Li et al., 2015; van der Merwe & Engelbrecht, 2003; Saatchi & Hung, 2005). Comparing the segmented images of existing methods with the proposed FFQOAK method, it is found that the proposed FFQOAK method properly segmented the infected regions in the extracted images. The segmented images obtained from the existing methods shown in Figs. 4–11(e)~(i), show that the existing methods cannot deal with these images as they have inconsistent and vague boundaries. On the other hand, the segmented images derived from the proposed FFQOAK method clearly highlight the infected regions and their boundaries.

Finally, a statistical analysis of the proposed and existing methods is performed using the MSE, PSNR, JSC and CC metrics. To simplify the comparison, the average values of MSE, PSNR, JSC and CC are considered. The proposed FFQOAK method is compared with the existing methods (Juang & Wu, 2010; Khrissi et al., 2020; Li et al., 2015; van der Merwe & Engelbrecht, 2003; Saatchi & Hung, 2005). Table 2 shows the results of the comparison in terms of average MSE values. The average MSE values of the four experimental sets, namely Experimental_Set_1, Experimental_Set_2, Experimental_Set_3 and Experimental_Set_4, obtained by KMC, GAK, PSOK, DPSOK, ACOK and the proposed FFQOAK method are 5293.23, 2203.31, 1844.26, 1305.61, 1136.73 and 712.30, respectively. These statistics show that the average MSE values of all these existing methods are much higher than the proposed FFQOAK method. Table 3 shows the results of the comparison in terms of average PSNR values. The average PSNR values of the four experimental sets obtained using KMC, GAK, PSOK, DPSOK, ACOK and the proposed FFQOAK method are 11.02, 14.70, 15.68, 17.01, 17.60 and 19.61, respectively. The comparison of these values shows that the proposed method has a higher PSNR value than the existing methods. Table 4 shows the average JSC values of the existing methods and the proposed FFQOAK method. For Experimental_Set_1, Experimental_Set_2, Experimental_Set_3 and Experimental_Set_4, the respective average JSC values obtained from KMC, GAK, PSOK, DPSOK, ACOK and proposed FFQOAK method are 0.37, 0.48, 0.74, 0.77, 0.84 and 0.90, respectively. These values show that the average JSC value of the proposed FFQOAK method is significantly higher than that of the existing methods. Table 5 shows the average CC values for the existing methods and the proposed FFQOAK method. From the four experimental sets, the average CC values for the KMC, GAK, PSOK, DPSOK, ACOK and proposed FFQOAK method are 0.43, 0.53, 0.68, 0.77, 0.84 and 0.91, respectively. These statistics show that the proposed FFQOAK method has a higher CC value than the existing methods. This statistical analysis shows that the proposed FFQOAK method outperforms the existing methods in segmenting the different regions of chest CT scan images of COVID-19 patients.

Table 4
Comparison of JSC with the existing methods and the proposed FFQOAK for the chest CT scan images of COVID-19.

Dataset	Case label	Extracted image	KMC	GAK	PSOK	DPSOK	ACOK	FFQOAK
Experimental_Set_1	1	#142	0.36	0.49	0.64	0.79	0.81	**0.88**
	2	#94	0.39	0.50	0.65	0.77	0.80	**0.87**
	3	#105	0.36	0.53	0.76	0.78	0.82	**0.89**
	4	#85	0.34	0.51	0.75	0.79	0.83	**0.90**
	5	#100	0.39	0.52	0.73	0.79	0.82	**0.89**
	6	#110	0.31	0.48	0.77	0.76	0.83	**0.90**
	7	#94	0.32	0.47	0.74	0.79	0.84	**0.89**
	8	#96	0.33	0.52	0.73	0.78	0.82	**0.89**
	9	#109	0.34	0.43	0.74	0.79	0.83	**0.90**
	10	#155	0.38	0.43	0.73	0.79	0.83	**0.90**
Experimental_Set_2	1	#118	0.38	0.48	0.78	0.79	0.89	**0.92**
	2	#106	0.38	0.48	0.75	0.78	0.84	**0.91**
	3	#81	0.39	0.41	0.74	0.79	0.82	**0.89**
	4	#71	0.39	0.49	0.72	0.76	0.86	**0.91**
	5	#76	0.38	0.48	0.75	0.79	0.82	**0.87**
	6	#87	0.39	0.41	0.76	0.76	0.88	**0.91**
	7	#113	0.37	0.42	0.74	0.78	0.87	**0.90**
	8	#120	0.40	0.47	0.75	0.77	0.82	**0.89**
	9	#90	0.39	0.46	0.76	0.79	0.83	**0.90**
	10	#179	0.39	0.45	0.74	0.78	0.84	**0.91**
Experimental_Set_3	1	#129	0.36	0.48	0.75	0.78	0.83	**0.90**
	2	#97	0.38	0.51	0.64	0.79	0.84	**0.91**
	3	#92	0.37	0.53	0.76	0.75	0.81	**0.88**
	4	#95	0.34	0.53	0.74	0.77	0.85	**0.91**
	5	#87	0.38	0.51	0.72	0.76	0.83	**0.90**
	6	#98	0.34	0.58	0.76	0.76	0.85	**0.91**
	7	#102	0.35	0.47	0.75	0.74	0.83	**0.90**
	8	#107	0.36	0.52	0.76	0.76	0.81	**0.89**
	9	#100	0.36	0.46	0.76	0.73	0.83	**0.90**
	10	#166	0.36	0.48	0.74	0.76	0.84	**0.91**
Experimental_Set_4	1	#136	0.36	0.49	0.73	0.78	0.86	**0.91**
	2	#86	0.37	0.47	0.75	0.79	0.83	**0.90**
	3	#100	0.40	0.45	0.74	0.78	0.81	**0.87**
	4	#77	0.38	0.47	0.73	0.76	0.87	**0.91**
	5	#80	0.39	0.46	0.76	0.79	0.83	**0.88**
	6	#92	0.39	0.47	0.75	0.76	0.86	**0.91**
	7	#89	0.36	0.43	0.74	0.77	0.87	**0.90**
	8	#114	0.40	0.46	0.73	0.78	0.85	**0.89**
	9	#104	0.36	0.47	0.74	0.79	0.82	**0.89**
	10	#171	0.37	0.46	0.75	0.77	0.85	**0.90**
Average	–	–	0.37	0.48	0.74	0.77	0.84	**0.90**

Based on the statistical analyses discussed above, it is obvious that the performance of the proposed FFQOAK method is better than the KMC algorithm. These analyses also indicate that the proposed FFQOAK method outperforms the existing hybridized methods, such as GAK, PSOK, DPSOK and ACOK.

5.4. Convergence analysis

The main reason of outperforming the proposed FFQOAK method is that FFQOA is more robust than GA, PSO, DPSO and ACO, which are hybridized with the KMC algorithm. In order to justify it, fitness of the GAK, PSOK, DPSOK and ACOK are evaluated. The main goal of the GAK, PSOK, DPSOK, ACOK and FFQOAK is to search the best fitness value for Euclidean distance function during the segmentation process of the chest CT scan images of COVID-19 patients. Table 6 presents outcomes of comparison in terms of average of best fitness values. To simplify the comparison, the average of the best fitness values is considered. The average of the best fitness values for Experimental_Set_1, Experimental_Set_2, Experimental_Set_3, and Experimental_Set_4 obtained from GAK, PSOK, DPSOK, and ACOK are 3.83×10^{-2}, 2.66×10^{-3}, 2.41×10^{-4} and 2.51×10^{-5}, respectively. However, the average of the best fitness value for Experimental_Set_1, Experimental_Set_2, Experimental_Set_3 and Experimental_Set_4 obtained by FFQOAK method is 3.17×10^{-7}, which is much lower than the existing methods, viz., GAK, PSOK, DPSOK and ACOK. This shows that the FFQOA is very effective compared to the selected optimization algorithms, i.e., GA, PSO, DPSO and ACO. Therefore, it improves the performance of the proposed FFQOAK method (especially the KMC algorithm) compared to the existing GAK, PSOK, DPSOK and ACOK methods.

To better understand the behavior of FFQOAK compared to the existing methods GAK, PSOK, DPSOK and ACOK in finding the best fitness value, the convergence curve analysis is performed. The convergence curves of the selected methods, including FFQOAK are shown in Figs. 12–15 for four experimental sets. From these figures, four different behaviors for the GAK, PSOK, DPSOK, ACOK and the proposed FFQOAK methods can be seen within 100 epochs:

Behavior I: It is observed that the FFQOAK method converges *very fast* in the entire search space compared to the GAK, PSOK, DPSOK and ACOK methods in terms of four experimental sets.

Behavior II: The FFQOAK converges *very well* to the search of the best fitness value with respect to four experimental sets.

Behavior III: The FFQOAK converges *very expressively* from the first steps of the epochs with respect to Experimental_Set_1

Table 5
Comparison of CC with the existing methods and the proposed FFQOAK for the chest CT scan images of COVID-19.

Dataset	Case label	Extracted image	KMC	GAK	PSOK	DPSOK	ACOK	FFQOAK
Experimental_Set_1	1	#142	0.40	0.50	0.65	0.74	0.81	**0.94**
	2	#94	0.41	0.51	0.66	0.75	0.82	**0.88**
	3	#105	0.41	0.51	0.66	0.75	0.82	**0.91**
	4	#85	0.40	0.50	0.65	0.74	0.81	**0.94**
	5	#100	0.40	0.50	0.65	0.74	0.81	**0.90**
	6	#110	0.42	0.52	0.67	0.76	0.83	**0.91**
	7	#94	0.42	0.52	0.67	0.76	0.83	**0.89**
	8	#96	0.45	0.55	0.70	0.81	0.88	**0.92**
	9	#109	0.44	0.54	0.69	0.80	0.87	**0.91**
	10	#155	0.42	0.52	0.67	0.78	0.85	**0.89**
Experimental_Set_2	1	#118	0.41	0.51	0.66	0.75	0.82	**0.89**
	2	#106	0.42	0.52	0.67	0.76	0.82	**0.92**
	3	#81	0.44	0.54	0.69	0.78	0.85	**0.90**
	4	#71	0.40	0.50	0.65	0.74	0.81	**0.89**
	5	#76	0.40	0.50	0.65	0.74	0.81	**0.89**
	6	#87	0.45	0.55	0.70	0.79	0.86	**0.90**
	7	#113	0.46	0.56	0.71	0.80	0.87	**0.91**
	8	#120	0.48	0.58	0.73	0.82	0.89	**0.93**
	9	#90	0.48	0.58	0.73	0.82	0.89	**0.93**
	10	#179	0.42	0.52	0.67	0.76	0.83	**0.90**
Experimental_Set_3	1	#129	0.42	0.52	0.67	0.76	0.83	**0.89**
	2	#97	0.41	0.51	0.66	0.75	0.82	**0.90**
	3	#92	0.43	0.53	0.68	0.77	0.84	**0.89**
	4	#95	0.40	0.50	0.65	0.74	0.81	**0.88**
	5	#87	0.41	0.51	0.66	0.75	0.82	**0.91**
	6	#98	0.42	0.52	0.67	0.76	0.83	**0.92**
	7	#102	0.46	0.56	0.71	0.80	0.87	**0.91**
	8	#107	0.45	0.55	0.70	0.79	0.86	**0.90**
	9	#100	0.44	0.54	0.69	0.78	0.85	**0.89**
	10	#166	0.42	0.52	0.67	0.76	0.83	**0.88**
Experimental_Set_4	1	#136	0.43	0.53	0.68	0.77	0.84	**0.90**
	2	#86	0.45	0.55	0.70	0.79	0.86	**0.92**
	3	#100	0.40	0.50	0.65	0.74	0.81	**0.94**
	4	#77	0.44	0.54	0.69	0.78	0.85	**0.95**
	5	#80	0.40	0.50	0.65	0.74	0.81	**0.93**
	6	#92	0.42	0.52	0.67	0.76	0.83	**0.95**
	7	#89	0.41	0.51	0.66	0.75	0.82	**0.92**
	8	#114	0.45	0.55	0.70	0.79	0.86	**0.93**
	9	#104	0.46	0.56	0.71	0.80	0.87	**0.95**
	10	#171	0.42	0.52	0.67	0.76	0.83	**0.92**
Average	–	–	0.43	0.53	0.68	0.77	0.84	**0.91**

compared to the GAK, PSOK, DPSOK and ACOK methods. This expressive convergence behavior is also observed for Experimental_Set_2, Experimental_Set_3 and Experimental_Set_4.

Behavior IV: It is observed that the GAK and PSOK methods are close to the local optimal fitness values in the case of four experimental sets. However, the DPSOK and ACOK methods show a small difference in finding the optimal fitness values compared to the GAK and PSOK methods. As shown in Figs. 12 and 15, the proposed FFQOAK method is able to search the optimal fitness values without getting into a local optimal situation compared to the GAK, PSOK, DPSOK and ACOK methods.

This analysis shows that the FFQOAK maintains the right balance between exploration and exploitation to find the best fitness values. From Figs. 12–15, it is also evident that the FFQOAK method is very competitive and has a high success rate compared to GAK, PSOK, DPSOK and ACOK methods in solving the clustering problem of chest CT scan images of COVID-19 patients.

5.5. Visual analysis of segmented images

A visual analysis is performed to evaluate the quality of segmented chest CT scan images of COVID-19 patients. The evaluation criterion is based on the ability to detect foreground and background regions and identify the infected regions. To demonstrate the visual analysis, segmented images obtained from KMC, GAK, PSOK, DPSOK, ACOK and proposed FFQOAK method are selected. To perform the clustering operation of each of the methods, the number of clusters is chosen as $\theta = 3$. For demonstration, some of the CT scan images are selected from four experimental sets. For visual analysis, the enhanced CT scan and the corresponding segmented images obtained by each method are cropped and enlarged to clearly show their features. Figs. 16–19(a) show the enhanced and enlarged CT scan images for Case labels 4 and 5. Segmented images obtained using the proposed FFQOAK method are shown in Figs. 16–19(b). For visual analysis, the segmented images obtained by the existing KMC, GAK, PSOK, DPSOK and ACOK methods are shown in Figs. 16–19(c)~(g), respectively. In Figs. 16–19(b), the white dense areas in the lungs show the signs and symptoms of COVID-19. Therefore, in Figs. 16–19(b), it can be seen that the proposed FFQOAK method produces better segmented images than KMC, GAK, PSOK, DPSOK and ACOK (Figs. 16–19(c)~(g), respectively).

Table 6
Comparison of the best fitness value with the existing methods and proposed FFQOAK in terms of segmenting the chest CT scan images of COVID-19.

Dataset	Case label	Extracted image	GAK × 10^{-2}	PSOK × 10^{-3}	DPSOK × 10^{-4}	ACOK × 10^{-5}	FFQOAK × 10^{-7}
Experimental_Set_1	1	#142	2.68	2.34	1.87	6.44	**2.66**
	2	#94	1.91	1.00	1.48	1.25	**3.83**
	3	#105	4.08	1.71	1.65	8.58	**1.02**
	4	#85	5.93	3.70	1.81	2.25	**2.12**
	5	#100	3.05	3.84	3.47	1.46	**2.66**
	6	#110	3.48	1.90	2.66	1.11	**2.20**
	7	#94	3.65	2.51	3.31	1.45	**1.24**
	8	#96	4.06	2.21	1.77	2.17	**3.36**
	9	#109	4.05	2.07	2.18	1.02	**1.40**
	10	#155	4.93	2.35	2.00	2.50	**6.38**
Experimental_Set_2	1	#118	4.00	1.06	2.78	3.24	**3.94**
	2	#106	2.11	1.00	1.18	1.77	**7.88**
	3	#81	3.40	4.07	3.02	1.64	**5.36**
	4	#71	3.97	2.83	2.27	1.23	**4.64**
	5	#76	5.40	1.91	4.07	2.33	**1.78**
	6	#87	4.00	5.05	1.92	1.16	**2.50**
	7	#113	5.69	5.51	2.37	2.59	**3.33**
	8	#120	3.13	3.95	2.00	1.83	**7.18**
	9	#90	5.69	3.75	3.61	1.16	**1.39**
	10	#179	4.14	3.95	2.00	1.83	**7.18**
Experimental_Set_3	1	#129	2.18	2.14	1.83	5.44	**2.16**
	2	#97	1.92	1.10	1.58	2.25	**3.93**
	3	#92	4.18	1.81	1.75	6.58	**1.12**
	4	#95	5.93	3.60	1.91	2.15	**2.22**
	5	#87	3.15	3.74	3.57	1.36	**2.86**
	6	#98	3.45	1.80	2.36	1.21	**2.40**
	7	#102	3.15	2.61	3.41	1.75	**1.14**
	8	#107	4.16	2.31	1.87	2.27	**3.46**
	9	#100	4.15	2.17	2.28	1.12	**1.20**
	10	#166	4.92	2.45	2.10	2.60	**6.48**
Experimental_Set_4	1	#136	1.18	2.64	2.83	4.44	**2.66**
	2	#86	2.62	2.10	1.68	3.15	**3.95**
	3	#100	4.38	1.91	1.75	4.58	**2.12**
	4	#77	4.93	3.50	2.91	3.15	**3.22**
	5	#80	4.15	2.74	3.87	2.16	**2.56**
	6	#92	4.45	2.10	2.86	1.61	**2.60**
	7	#89	3.25	2.81	2.71	1.45	**1.54**
	8	#114	3.86	2.31	2.67	2.57	**3.56**
	9	#104	3.95	2.97	2.38	1.62	**1.26**
	10	#171	3.92	2.75	2.50	2.10	**4.48**
Average	–	–	3.83	2.66	2.41	2.51	**3.17**

6. Conclusions and future directions

In this study, a new hybridized method, called FFQOAK was proposed. This method was based on the FFQOA and KMC algorithms. The proposed FFQOAK was applied to the segmentation of the chest CT scan images of COVID-19 patients. In the proposed method, KMC algorithm was used to segment the images while FFQOA algorithm was used to obtain the optimal segmented images. The proposed FFQOAK method was compared with the existing image segmentation methods, which include KMC, GAK, PSOK, DPSOK and ACOK. The performance of the proposed as well as the existing methods was evaluated using statistical metrics, such as MSE, PSNR, JSC and CC. The experimental results showed that the proposed FFQOAK method outperformed the existing methods. The empirical analysis showed that the proposed FFQOAK method not only preserved the advantages of the fast convergence ability of the KMC, but also solved its disadvantage of easily achieving an optimal local solution by using the FFQOA. Therefore, it can be concluded that the proposed FFQOAK method in this study was effective in analyzing the chest CT scan images of COVID-19 patients through the segmentation approach and proved to be an additional promising diagnostic method for medical experts.

The limitation of the study is that the proposed FFQOAK method was validated only with chest images. For future work, the proposed method can be improved to be applied to other types of medical images, such as X-rays and MRIs. In future, we will also try to demonstrate the application of the proposed FFQOA in solving various engineering design problems.

CRediT authorship contribution statement

Pritpal Singh: Conceptualization, Methodology, Validation, Reviewing and writing the article. **Surya Sekhar Bose:** Conceptualization, Methodology, Validation, Reviewing and writing the article.

Declaration of competing interest

The authors declare that they have no known competing financial interests or personal relationships that could have appeared to influence the work reported in this paper.

Ethical approval

This article does not contain any studies with human participants performed by any of the authors.

References

Berezin, F. A., & Shubin, M. A. (1991). *The Schrödinger Equation* (first ed.). The Netherlands: Kluwer Academic Publishers.

Cates, J. E., Whitaker, R. T., & Jones, G. M. (2005). Case study: an evaluation of user-assisted hierarchical watershed segmentation. *Medical Image Analysis*, *9*(6), 566–578.

Chan, J. F.-W., et al. (2020). A familial cluster of pneumonia associated with the 2019 novel coronavirus indicating person-to-person transmission: A study of a family cluster. *The Lancet*, *395*(10223), 514–523.

Chen, H., et al. (2020). Clinical characteristics and intrauterine vertical transmission potential of COVID-19 infection in nine pregnant women: A retrospective review of medical records. *The Lancet*, *395*(10226), 809–815.

Cheng, H., Jiang, X., Sun, Y., & Wang, J. (2001). Color image segmentation: advances and prospects. *Pattern Recognition*, *34*(12), 2259–2281.

Chung, M., et al. (2020). CT imaging features of 2019 novel coronavirus (2019-nCoV). *Radiology*, *4*, Article 200230.

Cohen, J., & Normile, D. (2020). New SARS-like virus in China triggers alarm. *Science*, *367*(6475), 234–235.

Douglas, S. C., & Losada, R. (2002). Adaptive filters in Matlab: from novice to expert. In *Proceedings of 2002 IEEE 10th Digital Signal Processing Workshop, 2002 and the 2nd Signal Processing Education Workshop* Pine Mountain, GA, USA: (pp. 168–173).

Fang, Y., et al. (2020). Sensitivity of chest CT for COVID-19: comparison to RT-PCR. *Radiology*, *19*, Article 200432.

Gordillo, N., Montseny, E., & Sobrevilla, P. (2013). State of the art survey on MRI brain tumor segmentation. *Magnetic Resonance Imaging*, *31*(8), 1426–1438.

Han, J., Yang, S., & Lee, B. (2011). A novel 3-D color histogram equalization method with uniform 1-D gray scale histogram. *IEEE Transactions on Image Processing*, *20*(2), 506–512.

Huang, Y.-P., Singh, P., & Kuo, H.-C. (2020). A hybrid fuzzy clustering approach for the recognition and visualization of MRI images of Parkinson's disease. *IEEE Access*, *27*, 25041–25051.

Huang, Y.-P., Singh, P., Kuo, W.-L., & Chu, H.-C. (2021). A type-2 fuzzy clustering and quantum optimization approach for crops image segmentation. *International Journal of Fuzzy Systems*, *23*(3), 615–629.

Huang, C., et al. (2020). Clinical features of patients infected with 2019 novel coronavirus in Wuhan, China. *The Lancet*, *395*(10223), 497–506.

Issac, A., Sarathi, M. P., & Dutta, M. K. (2015). An adaptive threshold based image processing technique for improved glaucoma detection and classification. *Computer Methods and Programs in Biomedicine*, *122*(2), 229–244.

Jourlin, M. (2016). Gray-level LIP model. Notations, recalls, and first applications. In M. Jourlin (Ed.), *Advances in Imaging and Electron Physics*: *vol. 195*, *Logarithmic Image Processing: Theory and Applications* (pp. 1–26).

Juang, L.-H., & Wu, M.-N. (2010). MRI brain lesion image detection based on color-converted K-means clustering segmentation. *Measurement*, *43*(7), 941–949.

Jun, M., et al. (2020). COVID-19 CT lung and infection segmentation dataset. http://dx.doi.org/10.5281/zenodo.3757476.

Katris, C. (2021). A time series-based statistical approach for outbreak spread forecasting: Application of COVID-19 in Greece. *Expert Systems with Applications*, *166*, Article 114077.

Khrissi, L., Akkad, N. E., Satori, H., & Satori, K. (2020). Image Segmentation Based on K-means and Genetic Algorithms. In *Embedded Systems and Artificial Intelligence* Fez, Morocco: (pp. 489–497).

Kong, B., et al. (2020). Learning tree-structured representation for 3D coronary artery segmentation. *Computerized Medical Imaging and Graphics*, *80*, Article 101688.

Levi, A. F. J. (2012). *Applied Quantum Mechanics* (second ed.). UK: Cambridge University Press.

Li, H., He, H., & Wen, Y. (2015). Dynamic particle swarm optimization and K-means clustering algorithm for image segmentation. *Optik*, *126*(24), 4817–4822.

Li, L., et al. (2020). Artificial intelligence distinguishes COVID-19 from community acquired pneumonia on chest CT. *Radiology*, *19*, Article 200905.

Manikandan, S., Ramar, K., Iruthayarajan, M. W., & Srinivasagan, K. (2014). Multilevel thresholding for segmentation of medical brain images using real coded genetic algorithm. *Measurement*, *47*, 558–568.

Menze, B. H., et al. (2014). The multimodal brain tumor image segmentation benchmark (BRATS). *IEEE Transactions on Medical Imaging*, *34*(10), 1993–2024.

van der Merwe, D. W., & Engelbrecht, A. P. (2003). Data clustering using particle swarm optimization. In *The 2003 Congress on Evolutionary Computation, Vol. 1* Canberra, ACT, Australia: (pp. 215–220).

Nowaková, J., Prílepok, M., & Snášel, V. (2017). Medical image retrieval using vector quantization and fuzzy S-tree. *Journal of Medical Systems*, *41*(2), 18.

Queen, J. M. (1967). Some methods for classification and analysis of multivariate observations. In *Proc. of the Fifth Berkeley Symposium on Mathematical Statistics and Probability, Vol. 1* Oakland, CA, USA: (pp. 281–297).

Saatchi, S., & Hung, C. C. (2005). Hybridization of the Ant Colony Optimization with the K-Means Algorithm for Clustering. In *Scandinavian Conference on Image Analysis* Joensuu, Finland: (pp. 11–520).

Schrödinger, E. (1935). The present status of quantum mechanics. *Die Naturwissenschaften*, *23*(48), 1–26.

Selim, S. Z., & Ismail, M. A. (1984). K-means-type algorithms: A generalized convergence theorem and characterization of local optimality. *IEEE Transactions on Pattern Analysis and Machine Intelligence*, *PAMI-6*(1), 81–87.

Singh, P. (2020a). A neutrosophic-entropy based adaptive thresholding segmentation algorithm: A special application in MR images of Parkinson's disease. *Artificial Intelligence in Medicine*, *104*, Article 101838.

Singh, P. (2020b). A neutrosophic-entropy based clustering algorithm (NEBCA) with HSV color system: A special application in segmentation of Parkinson's disease (PD) MR images. *Computer Methods and Programs in Biomedicine*, *189*, Article 105317.

Singh, P. (2021a). FQTSFM: A fuzzy-quantum time series forecasting model. *Information Sciences*, *566*, 57–79.

Singh, P. (2021b). A type-2 neutrosophic-entropy-fusion based multiple thresholding method for the brain tumor tissue structures segmentation. *Applied Soft Computing*, *103*, Article 107119.

Singh, P., Dhiman, G., & Kaur, A. (2018). A quantum approach for time series data based on graph and Schrödinger equations methods. *Modern Physics Letters A*, *33*(35).

Singh, P., Huang, Y. P., Chu, W. J., & Lee, J. H. (2020). A Fuzzy-Entropy and Image Fusion Based Multiple Thresholding Method for the Brain Tumor Segmentation. In *IEEE International Conference on Systems, Man, and Cybernetics (SMC)* Toronto, Canada: (pp. 2446–2451).

Singh, P., Huang, Y., & Lee, T. (2019). A novel ambiguous set theory to represent uncertainty and its application to brain MR image segmentation. In *IEEE International Conference on Systems, Man and Cybernetics (SMC)* Bari, Italy: (pp. 2460–2465).

Tobias, O. J., & Seara, R. (2002). Image segmentation by histogram thresholding using fuzzy sets. *IEEE Transactions on Image Processing*, *11*(12), 1457–1465.

WHO (2020). *Laboratory testing for 2019 novel coronavirus (2019-nCoV) in suspected human cases. Interim guidance*: *Technical Report*.

Xu, X., Xu, S., Jin, L., & Song, E. (2011). Characteristic analysis of Otsu threshold and its applications. *Pattern Recognition Letters*, *32*(7), 956–961.

Yang, X., Zhao, W., Chen, Y., & Fang, X. (2008). Image segmentation with a fuzzy clustering algorithm based on ant-tree. *Signal Processing*, *88*(10), 2453–2462.

Yao, H., Duan, Q., Li, D., & Wang, J. (2013). An improved K-means clustering algorithm for fish image segmentation. *Mathematical and Computer Modelling*, *58*(3–4), 790–798.

Zhou, P., et al. (2020). A pneumonia outbreak associated with a new coronavirus of probable bat origin. *Nature*, *579*, 270–273.

Zhu, N., et al. (2020). A novel coronavirus from patients with pneumonia in China, 2019. *New England Journal of Medicine*, *382*(8), 727–733.